JET–P(97)02

Critical Parameters for Turbulent Transport in the SOL: Mechanism for the L-H Transition and its impact on the H-mode Power Threshold and Density Limit in ITER

A V Chankin[1].

JET Joint Undertaking, Abingdon, Oxfordshire, OX14 3EA, UK.
[1] Permanent affiliation: Russian Scientific Centre “Kurchatov Institute”, INF, Moscow, Russia.

Preprint of a paper submitted for publication in
Plasma Physics and Controlled Fusion

January 1997

ABSTRACT

An explanation for the L-H transition through the electromagnetic mechanism: suppression of drift wave turbulence by the skin effect, is offered. In dimensional space, the bifurcation is attributed to the involvement of two parameters in the L-H transition physics: ρ^* and $\beta/\nu^*\rho^{*2}$ (the latter scales as aT^2 in physical parameters). Maximum of the diffusion coefficient, corresponding to the L-H transition, is reached when the *collisional* skin-depth $\Delta_{coll.skin} = \sqrt{c^2/8\sigma\nu}$ (ν - drift frequency) equals the characteristic radial displacement Δ of the drift turbulence. The same criterion can also be presented as: $D_\perp \equiv \Delta^2\nu = c^2/8\sigma$ - the condition for equal rates of the plasma diffusion into the magnetic field and the diffusion of the magnetic field into the plasma. The analysis yields the combination $T_e^{13/8}(T_e + T_i)^{3/8}/B(qR)^{1/4}$ (scales as $\left[\beta/\nu^*\rho^{*2/3}\right]^{3/4}$ in dimensionless parameters) as a critical parameter for the L-H transition, for the case of the $k_\perp\rho_s = const$ scaling for the wave vector of the drift turbulence. This threshold parameter should be applied near the separatrix position. A requirement that the *collisionless* skin-depth must be smaller than the radial displacement of the drift fluctuations in the L-mode, which is necessary for turbulence suppression, determines the threshold β for the L-H transition.

The proposed mechanism for the L-H transition clarifies the *R*-dependence of the H-mode power threshold: $P_{thres} \sim R^{1.75}$ scaling is predicted, with P_{thres}<70 *MW* for $\bar{n}_e = 5\times10^{19} m^{-3}$ in ITER. The critical parameter for the L-H transition, together with dimensionless parameters characterising pressure gradient and resistivity, create the set of similarity parameters describing ELM behaviour. The scaling for the separatrix density normalised to the Greenwald density limit $n_{e,sep}/n_{GW}$ with the machine size and toroidal field which ensures "similar" ELM behaviour can thus be obtained. For the fixed similarity parameters, the analysis yields weak ($\sim R^{1/4}$) but favourable dependence of $n_{e,sep}/n_{GW}$ on the major radius. In recent experiments on JET and other machines, the degradation in the edge confinement associated with increased ELM frequency was found to be responsible for the density limit in high power H-modes. Owing to the approximately $R^{1/4}$ dependence, an excess over the Greenwald limit, $\bar{n}_e/n_{GW}$, by about 30% higher in ITER compared to JET for "similar" conditions (q, $n_{e,sep}/\bar{n}_e$, separatrix z_{eff} and the T_e/T_i ratio, wall conditions, the use of pellets etc.) in ELMy H-modes is predicted. This is with the provision that a limit on the central density, related to mechanisms in the plasma core, is not encountered.

1. INTRODUCTION

It is widely accepted [1,2] that with the neglect of atomic processes and Debye scale events, the important dimensionless parameters of the tokamak discharge are:

$$\nu^* \sim \frac{nqR}{T^2}\ ,\ \ \rho^* \sim \frac{\sqrt{T}}{qRB}\ ,\ \ \beta \sim \frac{nT}{B^2}\ . \tag{1.1}$$

Fixing them ensures similar behaviour of the plasma in different conditions, irrespective of the machine size. These parameters are used for similarity studies in the main plasma. In the scrape-off layer (SOL), temperature and density are small, and, as was suggested by Lackner [3], β can be dropped as a similarity parameter. Instead, temperature must be fixed to correctly describe atomic processes, and the set of similarity parameters becomes:

$$\nu^* \sim \frac{nqR}{T^2}\ ,\ \ \rho^* \sim \frac{\sqrt{T}}{qRB}\ ,\ \ T. \tag{1.2}$$

The neglect of pressure effects related to β, as was pointed out in [3], may limit similarity of conditions in the two different machines: “since, perhaps not the physics in the scrape-off layer per se, but the form in which energy is ultimately fed into it might depend on β. This would clearly be the case in, for example, giant ELMs...” [3]. Following the work of Lackner, a discussion on the relative importance of similarity parameters in the SOL was carried out, notably by Hutchinson and Vlases [4], who proposed to pay attention to all of them, and by Catto et al. [5], who considered various specific models for physics in the divertor.

The present work is devoted to the analysis of physical mechanisms lying behind each of the similarity parameters. A dimensional approach can not only be applied to overall performance of the plasma but also to individual mechanisms (see e.g. Ref. [6] by Connor and Taylor). Attempts to apply the above mentioned parameters to describe intrinsic SOL processes, however, are complicated by the fact that the scrape-off layer has its own internal geometrical parameter. Even without neutrals, interaction with the target forces the width of the SOL to scale differently from the size of the machine: $\Delta_{sol} \sim (D_\perp qR/c_s)^{1/2}$. Unless the diffusion coefficient is specifically fitted to yield $\Delta_{sol} \sim qR$, the width of the scrape-off layer will not be proportional to qR. Therefore, physical mechanisms in the SOL are unlikely to be expressed through the above similarity parameters and some other combinations will have to be used.

Another difficulty in applying these parameters to the scrape-off layer originates from strong variation of plasma parameters across the SOL, often leaving its different parts in completely different situation with respect to the effectiveness of individual mechanisms in contributing to perpendicular transport. “Effective” mechanisms are those which, by their impact on either growth or suppression of the most important instabilities, determine the final state of strong turbulence with its characteristic frequencies and radial displacements. It appears to be that in the scrape-off layer there exist a number of very distinct conditions defined by corresponding domains of both plasma parameters and geometrical dimensions. They favour just a few “effective” physical mechanisms out of larger number of potential candidates. Conditions can be separated by specifying limits on certain combinations of the parameters. Such limits

may also be called critical parameters or thresholds. That is why, at least in the complex case of the SOL physics, it seems more appropriate to speak about critical parameters rather than similarity parameters in their usual sense. Not withstanding the above criticism, similarity parameters sometimes accurately reflect underlying physics even in the scrape-off layer, and at least may be used for initial separation of different conditions, before critical parameters are found.

As a starting point, the case of "cold" and "rare" SOL plasmas (low T and β, but not too high ν^*) is considered in this paper, for which transport scaling laws are derived (Section 2). For very low T, turbulence in such plasmas is strongly affected by collisionality (high ν^*). A lower limit on temperature as a function of other parameters, below which "typical" scaling laws in the SOL must break down, is determined in Section 3. Mechanisms limiting "low T low β physics", as these parameters are allowed to increase, are examined in Section 4. The effect of these limitations on the SOL transport, including MHD phenomena and the L-H transition, is discussed in Section 5. A comparison between threshold parameters associated with the proposed explanation for the L-H transition and local plasma parameters measured just inside the separatrix, is made in Section 6. Some aspects of dimensional similarity of discharges with an emphasis on simulation of perpendicular transport in the SOL are covered in Section 7. Experimental scalings for the H-mode power threshold are analysed in Section 8, where a dependence of the P_{thres} on major radius R which does not contradict to the proposed explanation of the L-H transition is derived. High T high β conditions reached near the separatrix in high input power high density discharges and their implication for overall discharge performance, in particular the possibility to exceed the Greenwald limit, are discussed in Section 9. The influence of the assumption that the decay length at the separatrix position scales with the scrape-off layer width Δ_{sol} on the main results obtained in this paper, and their modification in another limiting case where the decay length scales with the machine size, are examined in Section 10. Conclusions are formulated in the last section.

2. TRANSPORT IN THE "COLD" AND "RARE" SOL

In low β plasmas, only gradients of density and temperature (but not their product - pressure) can be a source of turbulence, which at very low temperatures implies collisional drift and interchange instabilities (see Section 3 and Appendix 1). The most universal instabilities are drift instabilities, both collisional and collisionless. For "cold" and "rare" plasmas (low T and β, but not too high ν^*) turbulence essentially consists of poorly correlated drift waves which interact with each other in their non-linear stage of development. Regardless of what causes growth of perturbations of electric potential, they will always behave like drift waves. This is roughly true even for the special case of an interchange instability affected by finite sheath conductivity [7,8], since perturbations of electric potential are proportional to T_e, as in the case of volume conductivity considered in the Appendix 1 (although the growth rates have different

dependencies on temperature). Therefore, to describe the most typical features of edge turbulence, the drift frequency should be selected as a characteristic frequency of fluctuations. This choice is justified by numerous experimental measurements of fluctuations at the edge [9].

Throughout this paper, the philosophy being followed is that whatever mechanisms contribute to the growth of the instability, the plasma will end up in a state of strong turbulence with short correlation times of the order of the inverse fluctuation frequency. The radial displacement of the plasma in the process of spatially de-correlated fluctuations will determine their characteristic wavelength λ_r (this is the basis for the so called "mixing length argument", applied to transport coefficients). Due to the possibility of the radial transfer of the fluctuation energy, turbulence may be non-local. The value of λ_r, and in many cases even its functional dependence on parameters, can only be obtained from experiment.

Strong turbulence with short correlation times τ_{corr} of the order of the inverse fluctuation frequency $1/\nu$ may cause problems for turbulence suppression by sheared E×B flows, the idea widely used in theories of the L-H transition (see e.g. [10-12]). The rate at which fluctuations are distorted by the sheared poloidal rotation associated with radially inhomogeneous radial electric field, $\nu_{shear} \approx d(cE_r/B)/dr$, may not be high enough to compete with the growth rate of perturbations when the growth rate of an instability γ is as high as the fluctuation frequency ν. The problem is aggravated in large machines (where ν_{shear} is lower) as was pointed out by Kotschenreuther, Dorland et al. (see e.g. [13] and refs. therein). However, as will be shown in Section 4, there may be other, electromagnetic mechanisms for turbulence suppression, which do not exhibit such a detrimental scaling with the machine size. One of them - the skin effect suppression of drift turbulence, is most likely to be responsible for the L-H transition. It yields a scaling for threshold parameters at the edge which roughly agrees with local measurements prior to the transition (Section 6).

Although the analysis which is presented here always refers to the diffusion coefficient $D_\perp$, similar arguments can generally be applied to χ_i. As for χ_e, analysis of perpendicular electron heat conductivity is complicated by the high parallel electron heat conduction that can smooth perturbations of T_e along the field lines. Also, since the SOL width is defined by both the perpendicular transport and the sink to the target, the effective width of the scrape-off layer with respect to the decay of electron temperature cannot easily be incorporated into the analysis owing to more complicated dependence of $\chi_{e\|}$ on T_e ($\sim T_e^{5/2}$) and the variability of the functional dependence of the electron heat sink at the target depending on the regime of transport (conduction or convection limits).

The plasma diffusion coefficient is defined by:

$$D_\perp = \Delta^2 \nu, \tag{2.1}$$

where Δ is a characteristic radial length of turbulent displacements, and ν - a characteristic frequency. For drift waves the characteristic angular frequency is given by:

$$\omega_d \equiv 2\pi\nu = k_\theta c T_e / eB\Delta_{sol} \ . \tag{2.2}$$

As for the functional dependence of k_θ and Δ (not to be confused with Δ_{sol}!), it cannot be established from first principles and has to be taken from experiment. Experiments indicate strong turbulence in the SOL with broad band frequency and wave vector spectra, with $k_\perp \rho_s$ being of the order of 0.2 [9]. For generality, however,

$$k_\perp \rho_s = f_{k\rho} \tag{2.3}$$

is adopted. For the Larmor radius, $\rho_s = c_s / \omega_i$ will be used, with $c_s = \sqrt{(T_e + T_i)/m_i}$. Other assumptions are conventional for drift turbulence. Large magnetic shear in the SOL ($q \sim r^2$) imposes a restriction on the minimum possible magnitude of the radial wave vector k_r (maximum λ_r) for given k_θ and $k_\parallel$, necessary for the very existance of the flux tube:

$$k_r / k_\theta = 2\pi / k_\parallel qR. \tag{2.4}$$

For the parallel wave vector, $k_\parallel = 1/qR$ ($\lambda_\parallel = 2\pi qR$) will be used, describing the longest most unstable fluctuations, which gives: $k_r / k_\theta = 2\pi$. In general, however,

$$k_r / k_\theta = f_{r\theta} \ , \tag{2.5}$$

so that one can trace the dependence on this parameter, but anyway, $f_{r\theta} > 1$. Values of $f_{r\theta}$ larger than unity are supported by observations. This allows one to replace $k_\perp = \sqrt{k_\theta^2 + k_r^2}$ with k_r, and the wave vectors are given by:

$$k_r = f_{k\rho} / \rho_s, \ k_\theta = f_{k\rho} / f_{r\theta} \rho_s \text{ and } k_\parallel = 2\pi / f_{r\theta} qR. \tag{2.6}$$

A radial displacement will be defined as:

$$\Delta = \lambda_r / 2 = \pi / k_r. \tag{2.7}$$

This is not in any way an arbitrary choice for the relation between Δ and k_r. It can be demonstrated that, provided turbulence is strong and fluctuations are de-correlated, the typical distance between maxima of density measured in microwave scattering experiments is, indeed, twice the average displacement.

With the above assumptions the angular frequency and radial displacement can be written as:

$$\omega_d = \frac{f_{k\rho}}{f_{r\theta}} \frac{T_e}{T_e + T_i} \frac{c_s}{\Delta_{sol}} \ , \tag{2.8}$$

$$\Delta = \pi \rho_s / f_{k\rho} \ . \tag{2.9}$$

The SOL width Δ_{sol} is found from:

$$\Delta_{sol} = (D_\perp \pi qR / M_\parallel c_s)^{1/2}, \tag{2.10}$$

where $M_\parallel$ is the Mach number of parallel plasma flow, to account for the possibility of strong recycling in the divertor, and the Eqs. (2.1), (2.2), (2.8) and (2.9):

$$\Delta_{sol} = \rho_s \left(\frac{\pi^2}{2 f_{k\rho} f_{r\theta}} \frac{T_e}{T_e + T_i} \frac{qR}{M_\parallel \rho_s} \right)^{1/3}. \tag{2.11}$$

This gives for ω_d:

$$\omega_d = \omega_i \frac{f_{k\rho}}{f_{r\theta}} \left(\frac{T_e}{T_e + T_i} \right)^{2/3} \left(\frac{2 f_{k\rho} f_{r\theta}}{\pi^2} \frac{M_\parallel \rho_s}{qR} \right)^{1/3}. \tag{2.12}$$

Finally, for the diffusion coefficient one obtains:

$$D_\perp = \frac{c_s \rho_s}{\pi} \left(\frac{\pi^2}{2 f_{k\rho} f_{r\theta}} \frac{T_e}{T_e + T_i} \right)^{2/3} \left(\frac{M_\parallel \rho_s}{qR} \right)^{1/3}. \tag{2.13}$$

The relation $D_\perp \sim T^{7/6} B^{-4/3} (qR)^{-1/3}$ following from this formula, is close to Bohm scaling against temperature and magnetic field, although it also contains a weak dependence on the machine size and q. It has to be emphasised that the only critical assumption required to obtain such a scaling is that $k_\perp \rho_s = const$. The other assumptions are conventional for drift turbulence.

Eq. (2.13) can be employed to estimate the magnitude of the diffusion coefficient. For easy comparison with the Bohm formula, $c_s \rho_s$ is replaced by $\frac{(T_e + T_i)(eV)}{B(T)}$ $m^2 s^{-1}$, whereas parameters inside brackets are kept fixed. Then, assuming $f_{k\rho} = 0.2$, $f_{r\theta} = 2\pi$, $q = 3$, $R = 3$ *m*, $M_\parallel = 1$, $T_e = T_i = 100$ *eV* and $B = 3$ *T* for fixed parameters, and the case of a deuterium plasma, Eq. (2.13) gives: $D_\perp = 0.042 \times \frac{T_e(eV)}{B(T)}$ $m^2 s^{-1}$, which is close to the Bohm diffusion coefficient ($1/16 \approx 0.063$).

As is clear from Eq. (2.13), the assumption $f_{k\rho} \equiv k_\perp \rho_s \sim \sqrt{\rho^*}$ is required to turn it into the exact Bohm-type scaling ($f_{r\theta}$ is not likely to change much as it is the longest perturbations along the field line that grow most rapidly; however, the exact value of this parameter is very uncertain once the plasma is already in the state of strong turbulence). The parameter $\sqrt{\rho^*}$ was varied widely across the experiments reviewed in the literature [9], enough to detect such a dependence. The fact that it has not been reported implies that $f_{k\rho}$ should be regarded as con-

stant. Still, the possibility of the $f_{k\rho} \sim \sqrt{\rho^*}$ scaling cannot be completely ruled out and will be used to provide an alternative scaling every time critical parameters are formulated. In contrast, a deviation in the opposite direction, $f_{k\rho} \sim 1/\sqrt{\rho^*}$, which would be difficult to justify physically, results in $D_\perp \sim T^{4/3}B^{-5/3}(qR)^{-2/3}$. It seems to exaggerate the dependence on the toroidal field and, therefore, will not be considered.

Scalings for Δ_{sol} and $D_\perp$ in the SOL and in the main plasma corresponding to different dependencies of $f_{k\rho} \equiv k_\perp \rho_s$ on ρ^*, ranging from being proportional to inversely proportional to this parameter, are assembled in Appendix 2. The $f_{k\rho} = const$ dependence corresponds to the gyro-Bohm scaling: $D_\perp \sim T^{3/2}/aB^2$, in the main plasma. It can be called a "local" scaling, since the fluctuation size in this case is proportional to a local parameter, the ion Larmor radius: $\lambda_\perp \sim \rho_s$. Another extreme case is Bohm-type scaling: $D_\perp \sim T/B \times qR/a$, corresponding to the $f_{k\rho} \sim \rho^*$ dependence. It may be called a "global" scaling, since the fluctuation size (or, rather, the radial correlation length of the turbulence spectrum) in this case scales with the size of the machine: $\lambda_\perp \sim qR$. The dependence of $D_\perp$ on q is eliminated when ρ^* is defined as $\rho^* \sim \sqrt{T}/RB$ instead of $\rho^* \sim \sqrt{T}/qRB$. There is a general understanding that "global" scaling describes energy confinement in the L-mode (low confinement regime) [14], whereas "local" scaling is responsible for energy confinement in the H-mode (high confinement regime) [15]. Large scale fluctuations are removed in H-mode plasmas. Underlying physical mechanisms for "local" and "global" scalings are discussed at the end of Section 5.

So far ν^*, being an important similarity parameter in the SOL physics (e.g. in parallel heat transport), did not figure in any equations. Conditions where it must be explicitly present in the equations related to turbulent transport, are considered in the next section.

3. THE CASE OF VERY LOW T (HIGH ν^*)

Collisional instabilities dominate in "very cold" plasmas. Mechanisms causing growth of perturbations are considered in Appendix 1, where a dispersion equation (A1.4) for the combined drift and interchange instability is derived. It has the form:

$$\omega^2 + i \cdot \alpha\omega\omega_d + i \cdot \omega\omega_s - i \cdot \omega_d\omega_s \pm \omega_o^2\left(k_y/k_\perp\right)^2 = 0 \ . \qquad (3.1)$$

Here $\omega_d = k_\theta cT_e/eB\lambda_n$ is the angular frequency of the drift wave, also responsible for the polarisation drift (ion inertia) giving rise to the drift instability; $\omega_o^2 = 2\left(T_e + T_i\right)/m_i R\lambda_n$ describes the effect of the vertical ∇B drift, leading to the interchange instability at the outer midplane (sign "+"), or stabilisation of turbulence at the inner midplane (sign "+"); $\omega_s = \omega_i\omega_e/\nu_{ei} \cdot k_\parallel^2/k_\perp^2$ characterises the ability of spatial charge to diffuse along the field lines

without creating perturbations of electric potential (proportional to ν_{ei}^{-1}); $\alpha = T_i/T_e$.

Expressions for wave vectors and results on Δ_{sol} from the previous section can be used to obtain the temperature and density dependence of the three main frequencies ($\lambda_n \equiv \Delta_{sol}$ is implied):

$$\omega_d \sim T^{1/6}, \;\; \omega_o\left(k_\theta/k_\perp\right) \sim T^{1/3}, \;\; \omega_s \sim T^{5/2}/n. \tag{3.2}$$

For the $f_{k\rho} \equiv k_\perp \rho_s \sim \sqrt{\rho^*}$ dependence, these results are slightly modified:

$$\omega_d \sim T^{1/4}, \;\; \omega_o\left(k_\theta/k_\perp\right) \sim T^{3/8}, \;\; \omega_s \sim T^{5/2}/n. \tag{3.3}$$

For relatively high temperatures (the criterion on T_e will be derived later in this section) the resistivity is small (high ω_s), and in the approximation $\omega_s >> \omega_d, \omega_o\left(k_\theta/k_\perp\right)$, corresponding to a small growth rate of the instability ($\gamma << \omega$), the dispersion equation (3.1) can be simplified:

$$\omega = \omega_d + i(\omega_d^2 \pm \omega_o^2 k_\theta^2/k_\perp^2)/\omega_s. \tag{3.4}$$

The imaginary parts of ω are the growth rates of the drift (symmetric part) and interchange (asymmetric part) instabilities. It is of interest to know their relative contributions to γ to assess which mechanism for instability is stronger: polarisation drift (drift instability) or ∇B drift (interchange instability). The equation $\omega_d = \omega_o k_\theta/k_\perp$ will define the transition between their relative strengths:

$$\frac{\rho_s}{qR} = \frac{1}{q^{3/2}} \frac{f_{k\rho}^3}{2\pi} \sqrt{M_\parallel f_{k\rho} f_{r\theta}} \left(\frac{T_e}{T_e + T_i}\right)^{5/2}. \tag{3.5}$$

From this equation, a temperature threshold above which the interchange instability will dominate can be obtained:

$$T_e + T_i = 1.22 \times 10^6 M_\parallel f_{k\rho}^7 f_{r\theta} \frac{m_i}{m_D} \left(\frac{T_e}{T_e + T_i}\right)^5 \frac{R(m)^2 B(T)^2}{q} \;\; eV. \tag{3.6}$$

For $T_e = T_i$, $f_{k\rho} = 0.2$, $f_{r\theta} = 2\pi$, $q = 3$, $R = 3\ m$, $M_\parallel = 1$, $B = 3\ T$ and $m_i = m_D$ it gives: $T_e = 41\ eV$. The exact figure is rather meaningless as the accuracy of the temperature prediction is lost in uncertainties of $f_{k\rho}$ due to the sensitivity to this parameter. Obviously, the ratio of growth rates of the two instabilities will make an impact on the in-out asymmetry of the diffusion coefficient. As a function of temperature, $\gamma_{interch.}/\gamma_{drift} = \omega_o^2 k_\theta^2/\omega_d^2 k_\perp^2$ is proportional to $T^{1/6}$. With such a flat temperature dependence and numerical uncertainties in the coefficients,

the dominant source of the instabilities cannot be quantitatively predicted.

Against temperature and density, $\gamma_{drift} = \omega_d^2/\omega_s$ scales as $n/T^{13/6}$ (n/T^2 for $f_{k\rho} \sim \sqrt{\rho^*}$). Therefore, at sufficiently high temperatures the growth rates become too small, and other, collisionless mechanisms will contribute to the instability. Various sources of instabilities will combine to create strong turbulence, and fluctuations will overlap, interact with each other and the charged particles, break up because of the shear etc. It is important to remember, however, that no matter what mechanism feeds the instability, it is (almost) always a drift wave which propagates and grows (or decays) in the plasma, so that all the results of the previous section, so far, are valid.

Restrictions on some of the assumptions made earlier occur at very low temperatures when the drift frequency ω_d becomes comparable with ω_s, and the growth rate of collisional instabilities approaches the frequency of oscillations. Physically, this corresponds to the situation where ion-electron friction becomes so efficient that the parallel current, compensating the charge pumped into a flux tube of length $\lambda_{||}/2 = \pi qR$ in the course of the oscillations, creates fluctuations of electric potential high enough to increase the growth rate of the instability up to $\gamma \approx Re\,\omega$. If the temperature is reduced even further, there will be no need for fluctuations to be so extended along the field lines, and they will become shorter. Shorter parallel wave length, owing to the shear restriction: $k_{||} = 2\pi/f_{r\theta}qR$ (Eqs. (2.4-2.6)), will imply smaller $f_{r\theta}$ ($1 < f_{r\theta} < 2\pi$) and a shorter poloidal wavelength (larger k_θ) for the same λ_r. The angular frequency of fluctuations $\omega_d = k_\theta cT_e/eB\Delta_{sol}$ will increase, resulting in an increase of $D_\perp$.

The critical condition for the plasma to become collisional from the standpoint of the development of instabilities, $\omega_d = \omega_s$, gives the equation:

$$\left(\frac{\rho_s}{qR}\right)^{5/3} = \frac{f_{k\rho}^2 M_{||}^{1/3}}{8}\left(\frac{2 f_{k\rho} f_{r\theta}}{\pi^2}\right)^{4/3}\left(\frac{T_e}{T_e+T_i}\right)^{2/3}\frac{\nu_{ei}}{\omega_e}. \qquad (3.7)$$

With $\nu_{ei} = 3.8\times10^{-11} z_{eff} n_e(m^{-3})[(T_e(eV)]^{-3/2}$ s^{-1} and $\omega_e = 1.76\times10^{11} B(T)$ s^{-1}, the electron temperature can be extracted as:

$$[T_e(eV)]^{7/3} = 8.1\times10^{-18} n_e(m^{-3}) z_{eff} M_{||}^{1/3} f_{k\rho}^{10/3} f_{r\theta}^{4/3}\left(\frac{m_i}{m_D}\right)^{5/6}\left(\frac{T_e}{T_e+T_i}\right)^{3/2}$$

$$\times [B(T)]^{2/3}[qR(m)]^{5/3}. \qquad (3.8)$$

For $n_e = 10^{19} m^{-3}$, $f_{k\rho} = 0.2$, $f_{r\theta} = 2\pi$, $q = 3$, $R = 3$ m, $M_{||} = 1$, $B = 3$ T, $z_{eff} = 1$ and $m_i = m_D$, this gives $T_e = 7.9$ eV. This temperature is much lower than the one corresponding to the boundary between the Pfirsch-Schlüter and Plateau regimes: $T_e = 134$ eV follows from the equation $\nu_{ei} = \sqrt{2T_e/m_e}/\pi qR$ for the above parameters.

The use of $\omega_d = \omega_s$ rather than $\omega_o k_\theta / k_\perp = \omega_s$ to determine the lower temperature collisional threshold was justified by the smallness of T_e (for $T_e = 7.9\ eV \quad \omega_d > \omega_o k_\theta / k_\perp$). Near and below this threshold, solutions of Eq. (3.1) have large growth rates. Solving Eq. (3.1) allows one to obtain the diffusion coefficient by applying the mixing length argument: $D_\perp \sim \gamma / k_r^2$, seeking the combinations of wave vectors yielding the largest $D_\perp$. Generally, the effect of shorter $\lambda_\parallel$ (smaller $f_{r\theta}$) will be to increase the diffusion coefficient given by Eq. (2.13) as the condition $\omega_d \approx \omega_s$ is approached. The degree of enhancement will depend on the collisionality. That is why ν^* is an important parameter for turbulent transport in strongly collisional plasmas.

4. LIMITATIONS ON DRIFT TURBULENCE ARISING FROM NON-ZERO β

Whilst ρ^* and ν^* are important parameters to describe turbulence in quasi-stationary magnetic fields in the $\beta \to 0$ approximation, finite β effects account for temporal evolution and small scale spatial variation of $\mathbf{B}$. There are three ways in which β comes into play in "cold" and "rare" plasmas: through a) the skin effect which may restrict turbulence, b) the microscopic electromagnetic fluctuations always accompanying drift turbulence, and c) MHD instabilities caused by the pressure gradient.

Fluctuations of the plasma with finite pressure generate fluctuating perpendicular currents according to $\nabla p = \frac{1}{c} \mathbf{j}_\perp \times \mathbf{B}$. Owing to the continuity equation: $div \mathbf{j} = 0$, $\mathbf{j}_\perp$ cause fluctuating parallel currents $\mathbf{j}_\parallel$, thereby introducing small scale perturbations of the magnetic field: $curl \mathbf{B}_\perp = \frac{4\pi}{c} \mathbf{j}_\parallel$, which enable electrons to move radially following the perturbed field lines (mechanism b)). If the parallel conductivity is high, however (high T_e), fast changes in $\mathbf{j}_\parallel$ will be impeded by the counter-current $\mathbf{E}_\parallel$ described by: $curl \mathbf{E}_\parallel = -\frac{1}{c} \frac{\partial \mathbf{B}_\perp}{\partial t}$. This is the essence of the skin effect and its possible suppression of turbulence (mechanism a)). In the equation $\frac{\partial \mathbf{B}}{\partial t} = curl(\mathbf{V} \times \mathbf{B}) + \frac{c^2}{4\pi\sigma} \Delta \mathbf{B}$ the skin effect is accounted for by the second term on the r.h.s., whereas the first term on the r.h.s. reflects changes in $\mathbf{B}$ due to the fast movement of the plasma across the magnetic field driven by the pressure gradient (mechanism c)).

The aim of this section is to find how limitations imposed on "low T low β physics" by these phenomena can be formulated and which ones occur first, as β is increased.

a) Skin effect

The skin frequency for the plasma column is: $\nu_{skin} = \frac{c^2}{4\pi\sigma a^2}$. Dividing it by the transit frequency $\omega_{tr} = v_e / qR$ gives a dimensionless parameter, which can be presented as:

$$\frac{\nu_{skin}}{\omega_{tr}} \sim \beta^{-1}\nu^{*}\rho^{*^2}(\varepsilon q)^{-1} \sim a^{-1}T^{-2}\ , \tag{4.1}$$

where $\varepsilon = a/R$. For given ν^* and ρ^*, finite β acts so as to reduce the skin frequency, or to increase the skin time. However, since the same ratio can also be expressed through T and minor radius a, from the physics' point of view, the skin effect is directly related not with β but with the plasma temperature. Large skin times restrict the radial extent and/or frequency of fluctuations. For fluctuations of radial size Δ, the relevant skin frequency can be obtained from the equation $\frac{\partial B}{\partial t} = \frac{c^2}{4\pi\sigma}\frac{\partial^2 B}{\partial r^2}$ ($k_r >> k_\theta$ is assumed), considering perturbations of the type $exp[i(\mathbf{kr} - \omega t)]$ with $k_r = \pi/\Delta$:

$$\nu_{skin} = \frac{c^2}{8\sigma\Delta^2}\ . \tag{4.2}$$

Drift turbulence, while being predominantly electrostatic, is nevertheless associated with fluctuating currents and magnetic fields that have the same temporal and spatial characteristics as the fluctuations of density and electric potential. These electromagnetic fluctuations are essential for the growth of perturbations (see Appendix 1). Small skin-depths introduce inhomogenities inside the flux tubes of the width of drift fluctuations Δ, causing their splitting into narrower tubes. For fluctuations of parallel current not to be restricted by the skin effect, the condition $\nu << \nu_{skin}$ must be satisfied, which leads to: $\Delta^2\nu << c^2/8\sigma$, or simply $D_\perp << c^2/8\sigma$.

Critical parameters for the onset of a strong influence of the skin effect on the drift turbulence can be found from the equation:

$$D_\perp = c^2/8\sigma\ . \tag{4.3}$$

$c^2/4\pi\sigma$ is often referred to as the diffusion coefficient for the penetration of the magnetic field into the plasma. Substituting $D_\perp$ from Eq. (2.13) into Eq. (4.3) gives:

$$c_s\rho_s = \frac{\pi}{8}\frac{c^2}{\sigma}\left(\frac{\pi^2}{2 f_{k\rho} f_{r\theta}}\frac{T_e}{T_e + T_i}\right)^{-2/3}\left(\frac{M_{||}\rho_s}{qR}\right)^{-1/3}\ . \tag{4.4}$$

Using $\sigma_{||} = 1.2\times10^{13} z_{eff}^{-1}(T_e(eV))^{3/2}\ s^{-1}$, the above criterion yields:

$$\frac{[T_e(eV)]^{13/6}[(T_e + T_i)(eV)]^{1/2}}{[B(T)]^{4/3}} = 1.9\times10^4 z_{eff} M_{||}^{-1/3}(f_{k\rho} f_{r\theta})^{2/3}\left(\frac{m_i}{m_D}\right)^{-1/6}[qR(m)]^{1/3}. \tag{4.5}$$

For $T_e = T_i$, $B = 3\ T$, $q = 3$, $R = 3\ m$, $M_{||} = 1$, $f_{k\rho} = 0.2$, $f_{r\theta} = 2\pi$, $z_{eff} = 1$ and $m_i = m_D$ one obtains: $T = 85\ eV$. For $T_i/T_e = 5$ it would give $T_e = 69\ eV$. Parameters $M_{||}$, $f_{k\rho}$, $f_{r\theta}$ and

z_{eff} may vary significantly. Variation of the toroidal field over the magnetic surface is also large. Some of the most unstable modes are located near the outboard of the magnetic surface. To stabilise these modes, the toroidal field B that has to be substituted into the Eq. (4.5), might need to be taken at a poloidal angle closer to the outboard rather than on the magnetic axis. This would especially make a strong difference in tight aspect ratio tokamaks by significantly reducing the threshold separatrix temperature required for the L-H transition. But even at the magnetic axis, the threshold T_e is lower in these machines since they have lower B for the same plasma current.

It is important to understand what physically happens to the drift fluctuations when the Eq. (4.3) is satisfied. As has already been mentioned at the beginning of this section, the skin effect is associated with an impedance to the flow of current along the field line which is necessary to compensate charges pumped into the flux tube. For low temperature drift turbulence these charges are pumped by the polarisation and ∇B drifts, and are also affected by the finite ion Larmor radius. The impedance to $j_{||}$ increases with the width of the flux tube and the parallel conductivity. For the same initial fluctuation $\tilde{j}_{||}$ (caused by the pumping of the charges into the flux tube by perpendicular non-ambipolar mechanisms), the induced counter-current parallel electric field following from the $\Delta E_{||} = 4\pi/c^2 \times \partial j_{||}/\partial t$ equation will result in the compensation of $\tilde{j}_{||}$ which would be proportional to the plasma conductivity $\sigma_{||} \sim T_e^{3/2}$.

Eq. (4.4) determines the critical temperature where the initial $\tilde{j}_{||}$ in the centre of the flux tube is fully compensated. The same equation can also be obtained by equalising the skin-depth $\Delta_{coll.skin} = \sqrt{c^2/8\sigma\nu}$ ($\nu = \omega_d/2\pi$ - drift frequency following from Eq. (2.12)) to the radial size of the drift fluctuations Δ given by Eq. (2.9). For higher temperatures, wide flux tubes (of the width Δ given by Eq. (2.9)) will break up into narrower ones, since the parallel current density will have a hollow profile across them. Small scale turbulence, owing to the square dependence of $D_\perp$ on the size of the fluctuations Δ, will reduce the diffusion coefficient. The advantage of formulating the skin effect as $\Delta^2\nu = c^2/8\sigma$, in its application to fluctuations of parallel current inside the flux tubes, is that it effectively imposes a "prohibition law" on combinations of Δ and ν which result in the diffusion coefficient $D_\perp = \Delta^2\nu$ being greater than $c^2/8\sigma$. Perturbations with larger products $\Delta^2\nu$ cannot develop.

b) Microscopic electromagnetic fluctuations

As was first pointed out by Callen [16], fluctuating parallel currents accompanying drift turbulence create micro-islands which cause electron heat flux. The amplitude of the fluctuations of the radial component of the magnetic field can be easily derived by substituting the contributions to $\tilde{j}_{||}$ found in Appendix 1, into the equations $curl\tilde{\mathbf{B}}_\perp = 4\pi\tilde{\mathbf{j}}_{||}/c$ and $div\tilde{\mathbf{B}}_\perp = 0$ ($k_r\tilde{B}_r + k_\theta\tilde{B}_\theta = 0$):

$$\tilde{B}_r \approx \frac{\beta}{2}\frac{k_\theta}{k_\parallel}\frac{\omega c}{c_s^2}\tilde{\varphi}\ , \tag{4.6}$$

where $\beta = 8\pi n(T_e + T_i)/B^2$ and $\tilde{\varphi}$ is the amplitude of fluctuations of the potential, of the order $T_e\Delta/e\Delta_{sol}$. The width of micro-islands can be estimated as:

$$\Delta_m \approx \frac{\tilde{B}_r}{B}\frac{\lambda_\parallel}{2} = \frac{\tilde{B}_r}{B}\frac{\pi}{k_\parallel}\ , \tag{4.7}$$

with an upper limit on the associated electron heat conductivity:

$$\chi_e = \Delta_m^2 \nu_{e_{tr}} = \Delta_m^2 \frac{2\pi}{f_{r\theta}}\frac{v_e}{\pi qR}\ . \tag{4.8}$$

This form of χ_e reflects the extreme case of a resonance where, after every passage along the parallel length $f_{r\theta}\pi qR/2\pi = \lambda_\parallel/2$ of the perturbations, electrons are shifted radially by Δ_m. For $v_e = \sqrt{T_e/m_e}$, using all the previous results, a critical β corresponding to the condition that this mechanism has a strong impact on the radial transport: $\chi_e = D_\perp$, can be derived:

$$\beta = \frac{2\pi}{f_{k\rho}^2\sqrt{M}}\left(\frac{2\pi}{f_{r\theta}}\right)^{1/2}\left(1+\frac{T_i}{T_e}\right)^{23/12}\left(\frac{m_e}{m_i}\right)^{1/4}\frac{\rho_s}{qR}\ . \tag{4.9}$$

For the parameters used earlier in numerical estimates this gives $\beta = 5.8\times10^{-3}$. A critical density $n = 6.5\times10^{20}\ m^{-3}$ follows from this criterion for $T_e = T_i = 100\ eV$ (if there was no resonance between $2v_e/\lambda_\parallel$ and ν, the density would be even higher). Against temperature and toroidal field, it scales as $n \sim B/\sqrt{T}$, and can hardly be reduced to the measured values at the separatrix by reducing B. Therefore, the density required to cause large χ_e is too high to be reached in experiments and such a microscopic electromagnetic turbulence should not contribute to radial fluxes in the SOL.

c) Pressure gradient as a source of MHD instabilities

Among the MHD phenomena caused by the pressure gradient, ELMs are of the greatest interest for edge physics. According to [17], resistive ELM activity begins if the critical value for β exceeds: $\beta = \frac{2R\Delta_{sol}}{L_\parallel^2}$, where $\beta = 8\pi n(T_e + T_i)/B^2$. Assuming $L_\parallel = 2\pi qR$ and substituting Δ_{sol} from Eq. (2.11) into this criterion, gives:

$$\beta = \frac{M_{\|}^{-1/3}}{2\pi^2 q}\left(\frac{\pi^2}{2 f_{k\rho} f_{r\theta}}\frac{T_e}{T_e + T_i}\right)^{1/3}\left(\frac{\rho_s}{qR}\right)^{2/3}. \qquad (4.10)$$

For the parameters used earlier $\beta = 3.8\times10^{-5}$. This threshold is substantially lower than the one derived in the previous sub-section. For $T_e = T_i = 100\ eV$ and $B = 3\ T$, $n = 4.3\times10^{18} m^{-3}$.

The value of β given by this criterion will not be used in the following analysis. Its functional dependence essentially states that the critical gradient of the poloidal beta near the separatrix is inversely proportional to the major radius: $\nabla\beta_\theta \sim 1/R$, where Δ_{sol} is used as a characteristic decay length. Such a dependence on R is typical for the MHD phenomena caused by the pressure gradient. For example, the Sykes-Troyon beta limit [18,19]: $\beta \sim I_p/aB$, can also be written as $\nabla\beta_\theta \sim q/R$, when the minor radius a is taken as a characteristic radial decay length.

The importance of the magnitude of β in MHD phenomena caused by pressure gradients comes eventually from the similarity of magnetic configurations. On the global scale, the Shafranov shift increases pressure gradients on the outboard side of the magnetic surface where the curvature of the field lines is unfavourable, resulting in ballooning instabilities. The Shafranov shift originates from the superposition of the poloidal magnetic fields created by the inductive (main) plasma current and the parallel Pfirsch-Schlüter current (which has opposite directions on the inboard and outboard sides of the magnetic surface) arising from the divergence of the diamagnetic current: $j_\theta \approx cp/aB$. The ratio of j_θ to the main parallel current density: $j_{\|} \sim B/qR$, which determines poloidal variation in spacing between the magnetic surfaces, can be expressed as:

$$j_\theta / j_{\|} \sim \beta \times q/\varepsilon\ . \qquad (4.11)$$

As for the two other dimensionless parameters: ν^* and ρ^*, they come from the similarity of parallel transport and drift motions. The ratio of collisional frequency $\nu_{coll} \sim nT^{-3/2}$ to transit frequency $\nu_{tr} \sim \sqrt{T}/qR$ gives:

$$\nu_{coll}/\nu_{tr} \sim nqR/T^2 \sim \nu^*\ . \qquad (4.12)$$

The ratio of the drift velocity $V_\theta = cE_r/B \sim T/aB$ (for the ∇B drift $V_\theta \sim T/RB$) to the parallel velocity $V_{\|} \sim \sqrt{T}$ gives:

$$V_\theta / V_{\|} \sim \sqrt{T}/aB \sim \rho^*\ . \qquad (4.13)$$

The parameter ρ^* accounts for the similarity of macroscopic drift motions and drift turbulence. The skin effect, according to Eq. (4.1), can be expressed by the parameter $\beta/\nu^*\rho^{*2}$. The involvement of two parameters in the dynamics of the turbulence creates the potential for a

bifurcation at some critical temperature. In dimensionless parameters, the criterion for the L-H transition (4.5) corresponds to a critical value of $\beta/\nu^*\rho^{*2/3}$.

In recent three dimensional computations of turbulence with the inclusion of electromagnetic effects by Scott et al. [20] and by Rogers et al. [21] it was found that the magnitude of β has strong influence of the state of the turbulence. Early indications in the model also containing profile dynamics [20] were that the turbulence should be moderately suppressed when β is increased to values above the electron/ion mass ratio:

$$\beta > m_e/m_i \ . \tag{4.14}$$

This parameter may be derived by equating the parallel electron velocity $v_e = \sqrt{T_e/m_e}$ with the Alfvén velocity $V_A = B/\sqrt{4\pi n m_i}$, pointing to a possible role of drift-Alfvén turbulence in the L-H transition; it is also the point at which the collisionless skin-depth, $c/\omega_{p_e} = c/\sqrt{4\pi n e^2/m_e}$, becomes as small as the drift scale, $\rho_s = \sqrt{T/m_i}/\omega_i$, so that all important scales of motion have an electromagnetic response in the electron parallel dynamics. When the profile effects are separated out, however, the turbulence itself actually becomes stronger with increasing β [21]. Whether the interaction of profile and turbulence dynamics gives a maximum in the transport, as in [20], but with the inclusion of more realistic profile effects, particularly in the scrape-off layer, must still be sorted out. Nevertheless, as will be shown in Section 6, a threshold in β is unlikely to be the parameter which controls the L-H transition. Local measurements inside the separatrix near the edge of the pedestal, where $\beta = m_e/m_i$ is often reached just prior to the L-H transition, indicate that the transition is mainly controlled by the critical T_e which increases with the toroidal field, whereas the dependence on density explicitly present in β is very weak, at least in typical medium to high density plasmas.

5. INFLUENCE OF HIGH T AND β ON THE SOL TRANSPORT: A MECHANISM FOR THE L-H TRANSITION

Analysis of limitations imposed by high T and β on intrinsic "cold" and "rare" SOL turbulence performed in the previous section, has revealed two main physical mechanisms: suppression of fluctuations by the skin effect and the appearance of the pressure gradient as an additional source of turbulence. The latter is responsible for ELMs. The criteria for conditions where these mechanisms become effective are given by Eqs. (4.5) and (4.10).

Suppose the temperature is raised above the threshold specified by Eq. (4.5). The plasma enters the regime where the radial extent and/or frequency of turbulent displacements is restricted by the skin effect and $D_\perp \approx c^2/8\sigma$. Since $\sigma \sim T_e^{3/2}$, the diffusion coefficient will decrease with temperature as $D_\perp \sim T_e^{-3/2}$. Such a trend is unlikely to continue up to a *keV* range

of temperatures, as new, e.g. MHD instabilities caused by both high β and large current density gradients, $\nabla j_{||}(r)$, pertinent to the hot core plasma, would develop. In certain range of temperatures, however, the decrease of $D_\perp$ with T_e is likely to be observed, leading to a bifurcation where the separatrix temperature, after it has reached the peak of the $D_\perp(T_e)$ dependence, can make a sudden upward excursion accompanied by a decay in the level of fluctuations. A decrease in $D_\perp$ will cause growth of T_e as a transport barrier is formed (it is implied here that χ_e will also decrease due to the reduced level of turbulence). The time scale for such an event is characterised by the speed of transport processes in a layer of the size of turbulent displacements, $\Delta = \pi\rho_s / f_{k\rho}$ (Eq. (2.9)). For the set of "typical" parameters used earlier, $\Delta = 1.07\times10^{-2} m$ for deuterium plasma ($\Delta_{sol} = 2.01 cm$ for this case; surface averaged widths are implied and the confinement regime is "bad" as expected from Bohm diffusion). Taking $D_\perp = 1.4\ m^2 s^{-1}$ which follows from Eq. (2.13) and is about 2/3 of the Bohm diffusion coefficient, gives: $\tau \approx \Delta^2 / D_\perp \approx 8\times10^{-5} s$. This is close to time scales for fast changes in the level of turbulence observed in experiment during the L-H transition. The degree of the increase in the separatrix temperature is difficult to predict. It requires the analysis of drift turbulence where the skin effect plays a role. Another restriction can be the influence of the MHD instabilities caused by both current density and pressure gradients (the latter is discussed below).

Lets look again at the criterion for suppression of drift turbulence by the skin effect (4.5). It can be recast as:

$$\frac{T_e^{13/8}(T_e+T_i)^{3/8}}{B} \sim (qR)^{1/4} \qquad \left(\frac{T_e^{13/6}(T_e+T_i)^{1/3}}{B} = const \ \text{ for } \ f_{k\rho} \sim \sqrt{\rho^*}\right). \qquad (5.1)$$

Owing to a very steep dependence of the parallel electron heat flow to the target on the electron temperature: $q_{e||} \sim T_e^{7/2} / L_{||}$, the T_e in the SOL, up to the separatrix position, must have a fairly weak (much weaker than linear) dependence on the input power. Therefore, a roughly square dependence on T_e inside the criterion (5.1) (which applies to the $f_{k\rho} \equiv k_\perp \rho_s = const$ scaling) does not necessarily contradict to the experimentally observed dependence of the H-mode power threshold on the toroidal field for constant density, which gives for the power flux through the separatrix: $P_{thres} / Sn \sim B$. More detailed analysis of the compatibility of the threshold (4.5) with the experimental H-mode power threshold will be carried out in Section 8. Comparisons between this threshold and measured local parameters, mainly T_e inside the separatrix, will be made in Section 6.

The skin effect can also provide an explanation for the radial profiles of χ_e in the SOL measured with Langmuir probes in both L- and H-mode discharges: χ_e appears to be lower near the separatrix (where T_e is higher) than deeper inside the SOL [22,23], contrary to the expectations based on Bohm formulae. This indicates possible strong influence of finite skin-depths on the size of fluctuations (or their correlation lengths) even in the L-mode, at least in the case of

the electron heat conductivity. There is also evidence for an inverse dependence of χ_e on the local T_e near the separatrix.

The influence of the pressure gradient on the SOL turbulence is manifested by a critical β in Eq. (4.10). It has the following parametric dependence:

$$\beta \sim T^{1/3}B^{-2/3}q^{-5/3}R^{-2/3} \qquad (\beta \sim T^{1/4}B^{-1/2}q^{-3/2}R^{-1/2} \quad \text{for} \quad f_{k\rho} \sim \sqrt{\rho^*}). \qquad (5.2)$$

For density, it gives:

$$n \sim T^{-2/3}B^{4/3}q^{-5/3}R^{-2/3} \qquad (n \sim T^{-3/4}B^{3/2}q^{-3/2}R^{-1/2} \quad \text{for} \quad f_{k\rho} \sim \sqrt{\rho^*}). \qquad (5.3)$$

The dependence on T is weakened by the $2/3$ power. Therefore, as a crude guidance, criterion (4.10) may be looked upon as a threshold for density. For very high densities, the effect of pressure gradient on the SOL may dominate over the effect of large skin times. Features typical of the H-mode may become less pronounced. It is likely that in these conditions coupling between drift and MHD turbulence occurs, dominated by the latter, as a result of which high frequency MHD turbulence driven by the pressure gradient (grassy ELMs?) may resemble drift turbulence, masking skin effect suppression, even when the criterion (4.5) is surpassed. This might explain experimental observations that in some discharges it is impossible to identify any sharp temporal changes in the character of the H_α fluctuations, as the discharge progresses from Ohmic to the L-mode phase (irregular fluctuations are seen on the H_α), then to the H-mode phase with grassy ELMs, then to distinct individual type I ELMs and, finally, to the ELM-free H-mode [24]. It is not excluded therefore that the decrease of $D_\perp$ with T_e may not take place at all in certain conditions and the dependence $D_\perp(T_e)$ is monotonic. These conditions are likely to be encountered when the parameter F_β which characterises pressure-gradient-driven instabilities (Section 9) is large.

In addition to the criterion (4.5) for suppression of drift turbulence by the skin effect which is related with Spitzer conductivity and determines the threshold for separatrix temperature (for given B), there is also one fundamental restriction on the very possibility for the *collisional* skin effect to suppress turbulence. It comes from the *collisionless* skin-depth originating from the residual plasma resistivity due to electron inertia and limits the maximum perpendicular wave vector $k_\perp$, so that distances shorter than certain value of $\lambda_\perp$ are beyond the control of the (*collisional*) skin effect. It is easy to show that for $k_r = \pi/\Delta$, radial turbulent displacements cannot be restricted by the skin effect if they are smaller than the collisionless skin-depth defined as $\Delta_{skin} = \pi c/\omega_{p_e}$. Numerically, this gives: $\Delta_{skin} = 1.67\times10^7/\sqrt{n_e(m^{-3})}$ *m*. For $n_e = 10^{19}m^{-3}$ this equals 0.53 *cm*. This distance has to be compared with a characteristic displacement of drift fluctuations: $\Delta_{drift} = \pi\rho_s / f_{k\rho}$. For $f_{k\rho} = 0.2$, $T_e = T_i = 100eV$, $B = 3T$ and deuterium plasma, this equals 1.07 *cm*. Therefore, $\Delta_{drift} > \Delta_{skin}$, and in this particular

example the skin effect does have the potential for reducing the size of fluctuations. For arbitrary plasma parameters the condition $\Delta_{drift} > \Delta_{skin}$ must be considered as necessary for suppression of turbulence. It can be formulated as:

$$\rho_s \omega_{p_e} > c f_{k\rho}, \tag{5.4}$$

and, owing to $\rho_s \sim \sqrt{T_e + T_i}/B$ and $\omega_{p_e} \sim \sqrt{n_e}$, can also be presented as a condition on minimum β:

$$\beta \equiv \frac{8\pi n(T_e + T_i)}{B^2} > 2\frac{m_e}{m_i} f_{k\rho}^2 = 2.19\times 10^{-5}\frac{m_D}{m_i}\left(\frac{f_{k\rho}}{0.2}\right)^2 . \tag{5.5}$$

For $T_e = T_i = 100eV$, $B = 3T$, $f_{k\rho} = 0.2$ and $m_i = m_D$ this gives for the threshold density: $n > 2.5\times 10^{18}\ m^{-3}$. The criteria (5.5) and (4.14) have the same parametric dependencies. However, for $f_{k\rho} = 0.2$ Eq. (5.5) gives a significantly lower β than the Eq. (4.14).

The dependence on temperature may be eliminated by combining inequality (5.5) with Eq. (4.5) (elevated to the power 3/8):

$$n > 3.2\times 10^{19} f_{k\rho}^{7/4} f_{r\theta}^{-1/4} M_{\|}^{1/8} z_{eff}^{-3/8}\left(\frac{m_i}{m_D}\right)^{-15/16}\left(\frac{T_e}{T_e + T_i}\right)^{13/16}\frac{[B(T)]^{3/2}}{[qR(m)]^{1/8}}\ m^{-3}. \tag{5.6}$$

This criterion may explain the existance of a lower density limit for the L-H transition observed in experiments. In typical discharge conditions this threshold should be exceeded for $f_{k\rho} = 0.2$ (it gives n>2.7×10^{18}m^{-3} for "typical" parameters used earlier), indicating that either $f_{k\rho} > 0.2$ or that the lower density limit is caused (or, at least, affected) by some other mechanisms (Section 7). Increase in the critical pedestal T_e often observed in experiments at low densities may be related with approaches to the density limit (5.6) when turbulent displacements in the L-mode phase prior to the L-H transition are close to the collisionless skin-depth. The electron parallel conductivity in these conditions is reduced by electrons' inertia, and higher T_e is required to cause the transition.

So far, in has been tacitly assumed that the L-H transition is triggered at the separatrix by virtue of it being the hottest point in the scrape-off layer. This argument, however, should make the plasma inside the separatrix an even more suitable location for triggering the L-H transition. There are nevertheless sufficient grounds to expect that it is the separatrix magnetic surface where the L-H transition is most likely to be triggered. The plasma as a whole, according to Kadomtsev [25], may be considered as a self-organising system which, through instabilities, is trying to reach the state of minimum free energy. Such a view is supported by experimental observations of profile consistency. Boundary conditions imposed on this system at the separatrix may come into conflict with internal mechanisms responsible for adjusting pressure and current

density profiles in the process of relaxation to the final state with optimum profiles. This is definitely the case when the plasma near the separatrix is “cold”. Sharp gradients of parallel current density, especially near the edge ($j_{||}$ is high in the plasma centre and almost zero - at the separatrix) cause the growth of tearing modes. A large number of non-linear tearing modes concentrated around magnetic surfaces with rational safety factor $q = m/n$ (but m and n numbers can be high!) will interact with each other, thereby generating magnetic noise all over the plasma.

This creates conditions for radial transfer of fluctuation energy across the plasma column, explaining fast re-adjustment of profiles. The tearing mode mechanism implies that the radial wave length of perturbations will scale with the machine size (for fixed m and n) giving rise to Bohm-type scaling (see Section 2). According to Kadomtsev, such an “incompletely relaxed” state of the plasma (provided it is “relaxed” with respect to a disruptive instability and ballooning modes) corresponds to the L-mode. This explanation of the nature of electron heat transport in the L-modes is supported by fast changes in χ_e observed in experiment during transient phenomena. As was concluded in Ref. [26] from the analysis of JET data: “During L-H and H-L transitions, χ_e is indirectly observed to change very rapidly close to the plasma edge and within a few milliseconds across most of the plasma... Similar changes to χ_e occur during ELMs and soft terminations. Collectively, these events represent anomalous L-mode transport switching on or off on a millisecond timescale.”

Solutions for $p(q)$ and $j_{||}(q)$ found in Ref. [25] for the case of good thermal insulation in the core (the H-mode), can only be realised for boundary conditions with a pedestal on the $j_{||}(q)$ profile. This can explain why high conductivity at the plasma edge is a pre-condition for existance of the H-mode. The H-mode is described as a state with “total relaxation to a minimum energy with current conservation”. Tearing modes do not grow into non linear stage with high amplitudes (or, at least, do not overlap), and plasma transport becomes “local” with gyro-Bohm scaling for transport coefficients.

An alternative (or additional) explanation for the strong profile consistency observed in both the L- and H-mode is provided by the idea of a critical temperature gradient [27,28,13] (the current density profile is, of course, closely related to the T_e profile). An empirical Rebut-Lallia-Watkins (RLW) model [28] assumes a strong increase in both χ_e and χ_i when the T_e gradient exceeds its critical value. In a series of calculations by Kotschenreuther, Dorland et al. (see [13] and refs. therein) core energy confinement was successfully reproduced by computations of toroidal ion-temperature-gradient-driven (ITG) turbulence. Increasing the T_i/T_e ratio was found to stabilise the ITG mode, resulting in better confinement. T_i profiles close to marginality (for the ITG turbulence) were found in H-modes, whereas in L-modes a significant deviation from critical profiles could occur, especially towards the edge. The core H-mode temperature was found to depend strongly on the pedestal temperature. These calculations, however, failed to

predict stabilisation of turbulence outside the edge of the pedestal, apparently due to the neglect of the effect of $\tilde{B}_\perp$ perturbations on $\tilde{E}_\parallel$.

Despite longer wavelength ITG modes being found to be unstable near the edge of L-mode plasmas, the ITG turbulence is mainly "local", with $k_\perp \rho_s \cong 1$ [13]. To explain Bohm-type confinement in L-mode, the scaling of $\lambda_\perp$ (or, rather, correlation length of turbulence) with the machine size is required. This can be provided by toroidal or non-linear coupling of the unstable modes (of any nature) [29,30]. The combination of "global" (i.e. with some dependence of $k_\perp \rho_s$ on R) transport at the edge with "local" ($k_\perp \rho_s \approx const$) transport in the core based on critical temperature gradient model was shown to correctly describe transient phenomena in JET [31]. Such a combination could explain both the Bohm-type global confinement and profile consistency in the L-mode.

There are two reasons why the separatrix position in particular should be regarded as the location where the L-H transition is likely to be triggered. Being the boundary between the two topologically different magnetic configurations (closed field lines inside it and open - outside), it should be prone to the maximum number of instabilities. Significant problems always occur when attempts to join solutions obtained inside and outside the separatrix are made. Outside the separatrix, particle and heat sinks towards the target cause poloidal non-uniformity of plasma parameters, whereas inside the separatrix profiles should be poloidally uniform. Satisfying the conditions for the suppression of turbulence near the separatrix should thus be sufficient for the whole plasma to switch into a state with better confinement.

Another reason to consider the separatrix as a favourable location for the L-H transition is the existence of short decay lengths of plasma parameters characteristic of the scrape-off layer. The criterion on the threshold temperature given by Eq. (4.5) was derived from the equation $D_\perp = c^2/8\sigma$. The diffusion coefficient is proportional to ω_d, which, in turn, has an inverse dependence on Δ_{sol}. Therefore, shorter decay lengths achieved at the separatrix compared to more inward positions facilitate the L-H transition by lowering the threshold temperature.

For the mechanism of drift turbulence suppression by the skin effect, the width of the transport barrier inside the separatrix observed in the H-mode (the so called "pedestal width": distance between the edge of the pedestal of temperature and density profiles and the separatrix) should be determined by the radial extent of the region where such suppression occurs. Further inside the main plasma, MHD instabilities in combination with drift, ITG etc. waves, are expected to determine the level of turbulence and the magnitude of transport coefficients.

6. LOCAL PARAMETERS AT THE L-H TRANSITION AS MEASURED IN EXPERIMENT

Equations (4.5), (5.5) and (5.6) give thresholds for separatrix temperature, β and density prior to the L-H transition that can be compared with experimental results. In recent experiments on

Alcator C-Mod [32], ASDEX Upgrade [33], DIII-D [34] and JET [35] detailed measurements of T_e near the separatrix have been carried out. However, due to mainly diagnostic limitations the data are presented not for the separatrix position but for an outer midplane position corresponding to 95% of the poloidal (Alcator C-Mod and ASDEX Upgrade) or toroidal (DIII-D) flux inside the separatrix, and for major radius corresponding to ≈95% of R_{sep} in JET. Since the criterion (4.5) for the L-H transition refers to the separatrix position, direct numerical comparison with the experimental data is impossible to make and only parametric dependencies can be compared.

In all four machines it is observed that edge T_e is the critical parameter for the L-H transition which supports the criterion (4.5). There is a limit for the T_e below which the transition cannot be obtained. The limit is the same for the L-H and H-L transitions, implying that the hysteresis in the input power (lower P_{input} is needed for the back H-L transition) often observed at medium densities is due to the improved confinement in the H-mode that establishes higher edge T_e.

The critical edge temperature increases with toroidal field in all four machines. The dependence $T_{e,edge} = f(B)$, however, is quite different from the one following from Eq. (4.5) for the $T_e = T_i$ case: $T_{e,sep} \sim \sqrt{B}$. Experiment gives $T_{e,edge} \sim B^{1.46}$ in Alcator C-Mod, $T_{e,edge} \sim B$ in ASDEX Upgrade and $T_{e,edge} \sim B^2$ in JET. The discrepancy between these results and the scaling prescribed by Eq. (4.5) is likely to originate from different locations of experimental data (inside the separatrix) and the separatrix position assumed in the Eq. (4.5). As has already been mentioned in Section 5, increase in separatrix temperature is severely restricted by steep dependence of electron heat sink to the target on T_e: $q_{e\|} \sim T_e^{7/2}/L_\|$. That is why separatrix T_e should be a rather flat function of the toroidal field in a sequence of discharges with increasing P_{input} which is necessary to cause the L-H transition.

In Alcator C-Mod, ASDEX Upgrade and DIII-D no dependence or very weak dependence of the critical $T_{e,edge}$ on q (or plasma current) is observed. That agrees well with the dependence of critical temperature following from Eq. (4.5). As for the dependence on density, almost no dependence of $T_{e,edge}$ on $\bar{n}_e$ is observed in Alcator C-Mod, unless the density is too small (see below). DIII-D note that there is an optimum $\bar{n}_e$ at which the L-H transition power threshold is lower, but the dependence on density is not strong. ASDEX Upgrade report the $T_{e,edge} \sim \bar{n}_{e,edge}^{-0.5}$ dependence. In JET, the dependence on the line average density along the chord corresponding to 93-94% of R_{sep} (well inside the pedestal) could be established. It was found to be very weak: $T_{e,edge} \sim (n_{e,edge})^{-0.083\pm0.152}$. Thus, taking all experimental facts into account, one has to conclude that the absence of explicit dependence on density of the criterion (4.5) should be regarded as one of its strong points.

Separately from the dependence of $T_{e,edge}$ on $\bar{n}_e$, stands the issue of lower density limit for the L-H transition. In Alcator C-Mod, no L-H transitions were observed for $\bar{n}_e < 9\times10^{19} m^{-3}$ in discharges with $B = 5.3$ *T*. Although part of the difficulties in obtaining H-modes in low density discharges is associated with higher input power required to raise $T_{e,edge}$, it is pointed out that "edge temperature threshold is a necessary but insufficient condition for remaining in H-mode, and that this local condition, unlike global power thresholds, does not show hysteresis" [32]. The density limit following from Eq. (5.6) would give $n_{e,sep} > 1.1\times10^{19}$ m^{-3} as a necessary condition for the L-H transition in this machine, lower than the expected $n_{e,sep} \approx \bar{n}_e/3 = 3\times10^{19}$ m^{-3}. The discrepancy can either be attributed to $f_{k\rho}$ being larger than 0.2 (due to sensitivity of Eq. (5.6) to this parameter, an assumption $f_{k\rho} = 0.36$ would bridge the gap between the two densities) or to some additional restraints related to the usual difficulties in obtaining very low density plasmas. For example, DIII-D report that at low densities, locked modes can raise the power threshold for the H-mode or even inhibit it. As was pointed out in the previous section, increase in the critical pedestal T_e observed in experiments at low densities may be related with approaches to the density limit (5.6) when turbulent displacements in the L-mode phase prior to the L-H transition are close to the collisionless skin-depth. The electron parallel conductivity in these conditions is reduced by electrons' inertia, and higher T_e is required to cause the transition.

The dependence of local parameters prior to the L-H transition on the toroidal field direction has been studied in Alcator C-Mod. It confirmed earlier observations on ASDEX Upgrade that in reversed B_t plasmas the edge electron temperature required to cause the L-H transition is substantially higher than in normal field ones. In Alcator C-Mod, threshold $T_{e,edge}$ was found to be approximately twice the threshold values with the normal B_t direction. This seems to contradict the explanation of the L-H transition through turbulence suppression by the skin effect, or at least to suggest that some other mechanisms affecting the transition are involved. However, in can also be argued that an extra power pinch near the separatrix expected in the normal B_t configuration compared to the reversed B_t one, due to neoclassical toroidal effects [36], will specifically affect the separatrix temperature, so that there must be a difference in the $T_{e,sep}$ in the two field configurations for the same $T_{e,edge}$ measured at the $\psi = 0.95$ surface.

In addition, such an extra pinch or outward flow (depending on the field direction) which also exists for particle fluxes [37], could affect the scrape-off layer width Δ_{sol}, thereby changing the criterion on the threshold temperature given by Eq. (4.5) so as to explain experimental trends. This criterion was derived from the equation $D_\perp = c^2/8\sigma$. Since the diffusion coefficient is proportional to ω_d, which, in turn, has an inverse dependence on Δ_{sol}, sharper gradients in the normal B_t configuration would result in a lower threshold temperature for the L-H transition.

A possible importance of the separatrix region in establishing conditions for the L-H transition is mentioned in the paper from Alcator C-Mod: "... since up-down asymmetries mainly affect the region outside or just inside the separatrix, the results of reverse field experiments imply that the extreme edge region plays an important role in H-mode physics"[32].

Regarding the sensitivity of the L-H transition threshold to dimensionless parameters, data from all four machines suggest that ν^* is not an important parameter. In the L-mode, just prior to the L-H transition, ν^* varied from 1.4 to 5 in ASDEX Upgrade and - from 2 to 17 in DIII-D. Alcator C-Mod note that, due to wide variation in ν^* and weak dependence of the $T_{e,edge}$ on density, "... ν^* and β are not important variables, or that their functional dependencies are such as to cancel out the density dependence" [32]. The mechanism of the skin effect suppression of drift turbulence suggests a different explanation. The dimensionless parameter characterising collisional skin effect is roughly proportional to the combination $\beta\varepsilon q\rho^{*-2}\nu^{*-1}$ (Eq. (4.1)). Therefore, irrespective of possible separate evolution of β and ν^* in the experiment, the density contribution is cancelled out.

7. DIMENSIONAL SIMILARITY OF TRANSPORT IN THE SOL AND DIVERTOR

Having established scaling laws for the most important mechanisms which influence turbulence in the SOL, it is worth re-examining the validity of arguments usually used for dimensional similarity of tokamak discharges. Strictly speaking, exact similarity means fixing ρ^*, ν^* and β. This makes the problem of simulation of an ITER discharge problematic due to its large size and toroidal field, as it requires:

$$B \sim (qR)^{-5/4}, \quad n \sim (qR)^{-2}, \quad T \sim (qR)^{-1/2}. \tag{7.1}$$

Geometrical parameters such as toroidicity $\varepsilon = a/R$, as well as safety factor q, must also be fixed because they influence transport. For purposes of restricted similarity it is, however, important to know how sensitive various mechanisms are to variation of the dimensionless parameters.

First, the drift turbulence as a fundamental feature of the "cold" and "rare" SOL. The scaling for the angular frequency of drift waves ω_d gives for a relevant dimensionless parameter, namely its ratio to the transit time: $\omega_d/\omega_{tr} \sim (\rho^*)^{-2/3}$, provided $k_\perp\rho_s = const$. This assumption leads to the $D_\perp \sim T^{7/6}B^{-4/3}(qR)^{-1/3}$ scaling for the diffusion coefficient, which is not far from the Bohm scaling. An insistence on the exact Bohm scaling would require $k_\perp\rho_s = \sqrt{\rho^*}$; then $\omega_d/\omega_{tr} \sim (\rho^*)^{-5/6}$. As reality must be somewhere between these two possibilities, ρ^* in any case emerges as the most important parameter for transport simulation in the

"cold" and "rare" SOL.

In "very low T" plasmas collisionality becomes important, and the question is whether ν^* correctly represents its influence on the transport. This appears to be the case. The ratio of growth rates of interchange and drift instabilities $\omega_o^2 k_\theta^2 / \omega_d^2 k_\perp^2$ is proportional to q, for fixed ρ^*. Fixing q, therefore, is a necessary condition for reproducing transport in collisional plasmas.

Complete similarity of turbulence in "cold" and "rare" SOL plasmas requires proportionality between the three frequencies determining the dynamics of the combined drift and interchange instability (Section 3):

$$\omega_d \sim \omega_o \sim \omega_s . \tag{7.2}$$

Provided toroidicity ε is also fixed, this would ensure that such a combined turbulence behaves in exactly the same way in all machines, with the same mode numbers etc. As another ratio, ω_d / ω_s, is proportional to $\nu^* \rho^{*3}$, ν^* must be fixed too. Thus, all four parameters: ρ^*, ν^*, ε and q, must be fixed to simulate turbulence of "cold" and "rare" plasmas. This would also ensure similarity of parallel transport, e.g. proportionality between parallel heat flux in the SOL and heat transmission through the Debye sheath, as well as similarity of instabilities affected by finite sheath conductivity. Proportionality between Δ_{sol} and qR and similar behaviour of macroscopic drift motions would also be observed.

Virtually all aspects of transport in the "cold" and "rare" SOL (except for the interaction with neutrals and other atomic processes, of course) can be simulated by fixing ρ^*, ν^*, ε and q. It becomes clear that the set of similarity parameters proposed by Lackner [3] (temperature also fixed) ensures complete similarity of the SOL behaviour including atomic processes, provided the plasma is "cold" and "rare". However, even if temperature is relaxed (atomic processes are ignored), the realistic possibility to simulate plasma transport in ITER using JET as a model can be questioned, as it implies: $T \sim q^2 R^2 B^2$, $n \sim q^3 R^3 B^4$, and both temperature and density in JET will have to be made too low.

This gives weight to the proposal made by Hutchinson and Vlases [4] to allow variation of the safety factor q (to raise it in a smaller "model" of the "reactor"). For strongly collisional plasmas, however, proportionality between growth rates of drift and interchange instabilities would require keeping q fixed. But in plasmas which are not too collisional, typical of the main SOL region, the priority given to the exact simulation of the combined drift and interchange instability is somewhat lower. As for the correct simulation of parallel transport, it is also affected by atomic physics, especially in high recycling plasmas. Accuracy in reconstructing details of parallel profiles has already been compromised by the exclusion of atomic processes. Thus, q and ν^* should be considered as a second-tier parameters, right after ρ^*, according to their importance in perpendicular transport in a SOL which is not too collisional. Unfortunately,

arguments have to be reversed again when transport in the divertor region is taken into consideration. There the plasma is too collisional for the regimes of practical interest (for the present reactor concept), and fixing parameters proposed by Lackner [3] (with the exception of T) has to be rigorously enforced in order to simulate transport in both SOL and divertor. However, similarity of atomic processes will be completely lost, as it requires a dramatic reduction in density and temperature.

Practical steps in modelling the "reactor SOL" would be: running a code for the "reactor" (assuming plasma-wall interactions and atomic processes can be correctly described) in which transport coefficients (ideally, local ones) are derived from experiments on the "model" in very low power and density discharges. $D_\perp$ obtained in the experiments should be scaled according to $D_\perp \sim \nu\Delta^2 \sim \omega_d R^2 \sim T/B$ (the same q in the "model" and "reactor" is assumed) when substituted into the "reactor" code. Owing to the $T \sim R^2 B^2$ proportionality which has to be adhered to in order to create similar conditions in the two machines, the experimental diffusion coefficient should be scaled up according to $D_\perp \sim R^2 B$ when substituted into the "reactor" code. A potential difficulty in creating similar conditions in the two machines stems from the fact that fluctuations tend to cover $\approx \pi q R$ distance along the field line. In this sense they are "global", and the same poloidal variation of plasma parameters in the "model" as in the "reactor" would ideally be required. This may prove to be unachievable. For example, it may be impossible to obtain detached plasma in the "model" for parameters relevant to similarity of the turbulence.

The way β should be treated for purposes of transport simulation depends on the regime of operation to be explored. In low density high power discharges affected by the density threshold for the L-H transition (5.6), β will be an important parameter, as this threshold is essentially the threshold on β. At higher density, proximity to the L-H transition, characterised by criterion (4.5), will provide a relevant similarity parameter for the ELM-free H-mode. At even higher densities, simulation of the MHD activity caused by the pressure gradient, according to Eq. (4.10), would require observing the proportionality $\beta \sim \rho^{*2/3}$. Thus, conditions expressed by Eqs. (4.5), (4.10) and (5.5), with one of them not exactly being related to β owing to specific details of the radial profiles in the SOL and a possibility that T_e and T_i may differ significantly, should be given certain weighted factors depending on the regime. In the core the situation would have been much easier, as the proportionality $\beta \sim \nu^* \rho^{*2} \varepsilon^{-1} q^{-1}$ correctly characterises the skin effect.

Finally, in radiative divertor experiments in the L-mode, atomic processes are likely to be as important as plasma parameters, and ρ^*, ν^*, q and T all have to be taken into account. At the same time, skin effect and MHD activity play no role in low T plasmas (the latter - only if $\beta/\rho^{*2/3}$ is small).

8. SCALINGS FOR THE H-MODE POWER THRESHOLD

Eq. (4.5) which gives the criterion for the suppression of drift turbulence by the skin effect and is related to the L-H transition, can be checked for consistency with the experimentally found dependence for the H-mode power threshold. In line with the dimensional approach adopted in this paper, the threshold power should scale as:

$$P_{thres} \sim R^2 \times nD_\perp (T_e + \alpha T_i)/\Delta_{sol} \ . \tag{8.1}$$

Coefficient α is mainly used to distinguish the $(T_e + \alpha T_i)$ combination from $(T_e + T_i)$ which enters ρ^* (present inside $D_\perp$ and Δ_{sol}). Since the heat conductivities χ_e and χ_i are not considered, the ratio $\alpha T_i / T_e$ describes the sharing of the power flux through separatrix between ion and electron channels.

Substituting the expressions for the diffusion coefficient $D_\perp$ and the scrape-off layer width Δ_{sol} found in Section 2 (Eqs. (2.13) and (2.11)) for the case of $f_{k\rho} \equiv k_\perp \rho_s = const$, results in:

$$P_{thres} \sim nR^2 (T_e + \alpha T_i)(T_e + T_i)^{1/2} T_e^{1/3} B^{-2/3} (qR)^{-2/3} \ . \tag{8.2}$$

This scaling has to be compared with the experimentally observed power threshold, which approximately has the form:

$$P_{thres} \sim nBR^\gamma . \tag{8.3}$$

There is a significant degree of confidence in the linearity of the dependence of P_{thres} on B, as well as the absence of a strong dependence on q. At the same time, the value of γ can only be established with a large scatter: $\gamma = 1.5 - 2.5$, as it involves comparison between different machines with different magnetic configurations, wall conditions etc. As for the dependence on density, experimental scalings are usually presented against the line average density $\bar{n}_e$. As the best fit to the multi-machine database on the power threshold, the ITER Confinement Database and Modelling Expert Group has adopted the following dimensionally correct scaling [38]:

$$P_{thres} = 0.45 \times B(T)(n_{20})^{0.75} [R(m)]^2 \times \left[0.6(n_{20})R(m)^2\right]^{\pm 0.25} MW, \tag{8.4}$$

where $n_{20} \equiv \bar{n}_e(m^{-3})/10^{20}$. It predicts $P_{thres} = 50 - 200\ MW$ for $\bar{n}_e = 0.5 \times 10^{20} m^{-3}$. With such a large uncertainty in the P_{thres} prediction, better knowledge of the R -dependence is crucial for ITER.

Against the line average density, the dependence $P_{thres} \sim \sqrt{\bar{n}_e}$ has been reported from JT-60U [39]. According to Eq. (8.4), it implies the $P_{thres} \sim R^{1.5}$ dependence on the major radius, which is very favourable for ITER as it yields 53 MW for $\bar{n}_e = 0.5 \times 10^{20} m^{-3}$. Recent

JET data, on the other hand, are best fitted by the $P_{thres} \sim \bar{n}_e^{0.75}$ dependence [35], corresponding to $P_{thres} \sim R^2$.

There is no simple relationship between the separatrix density and the line average density. It is usually assumed that $n_{sep}/\bar{n}_e \approx 3$, but significant deviations from this relation may occur. For the purposes of testing the criterion for the onset of the L-H transition given by Eq. (4.5), on the consistency with the experimental power threshold, the latter will be assumed to have the form (8.3) where n is understood to be the separatrix density, and no attempts to correct the density dependence will be made. Recent data from JET are in a very good agreement with the linear dependence of P_{thres} on the edge density: $P_{thres} \sim (n_{e,edge})^{0.952\pm0.089}$ [35].

The ratio of the two power thresholds, (8.2) and (8.3), which can be expressed as:

$$F_P \sim R^{2-\gamma}\left[\frac{(T_e+\alpha T_i)^{0.6}(T_e+T_i)^{0.3}T_e^{0.2}}{B(qR)^{0.4}}\right]^{5/3}, \qquad (8.5)$$

must be independent of plasma parameters, magnetic configuration and the machine size, provided the relation between these parameters correctly describes conditions prior to the L-H transition. Skin effect mechanism for the L-H transition roughly satisfies this criterion, since for the case of $k_\perp \rho_s = const$ it can be presented in the form: $\frac{T_e^{1.63}(T_e+T_i)^{0.37}}{B(qR)^{0.25}} = const$ (Eq. (5.1)), which follows from Eq. (4.5) and is close to the combination inside the square brackets of F_P. This mechanism can explain the absence of q dependence (with an insignificant difference $\sim q^{0.15}$ which contributes $q^{-1/4}$ dependence to F_P that should be ignored) provided $(T_e+\alpha T_i)^{0.6}(T_e+T_i)^{0.3}T_e^{0.2}$ scales as $T_e^{1.63}(T_e+T_i)^{0.37}$ over the range of machine/regime parameters which contributed to the $P_{thres} \sim nBR^{\gamma}$ scaling. For $\alpha = 1$, this requires $T_e \sim (T_e+T_i)^{0.37}$ proportionality, which seems probable as in the regimes with high edge temperatures typically $T_i >> T_e$, as invoked from the comparison between the power deposition onto the target measured with IR thermography and calculated power deposition from Langmuir probes which measure T_e and particle flux (see e.g. [40]). As for the dependence on major radius, $\gamma = 1.75$ is required to make F_P independent of R.

For the alternative ρ^* scaling of the perpendicular wave vector, $k_\perp \rho_s \sim \sqrt{\rho^*}$, $F_P \sim R^{2-\gamma}\left[\frac{(T_e+\alpha T_i)^{0.67}(T_e+T_i)^{0.28}T_e^{0.22}}{B(qR)^{0.33}}\right]^{3/2}$. This has to be compared with the condition $\frac{T_e^{2.17}(T_e+T_i)^{0.33}}{B} = const$ (second in Eq. (5.1)). The discrepancy with the scaling against q

inside the square brackets, $\sim q^{0.33}$, is larger than in the previous case, contributing $q^{-1/2}$ dependence to F_P which seems significant. However, if $\sqrt{T_e + T_i}/RB$ is used for ρ^* rather than $\sqrt{T_e + T_i}/qRB$, then the q-dependence inside F_P will change: $F_P \sim R^{2-\gamma}\left[\frac{(T_e + \alpha T_i)^{0.67}(T_e + T_i)^{0.28} T_e^{0.22}}{Bq^{0.44} R^{0.33}}\right]^{3/2}$. As for the L-H transition threshold, it will take the form: $\frac{T_e^{2.17}(T_e + T_i)^{0.33}}{Bq^{0.33}} = const$, and the difference in q-dependencies between the two expressions almost disappears. An explanation of the L-H transition through the skin effect would require $\gamma = 1.5$ in order to make F_P independent of R.

Finally, the $k_\perp \rho_s \sim \rho^*$ dependence yields $\gamma = 1.0$, which is in a clear disagreement with the R-dependence of the experimental H-mode power threshold. Therefore, the possibility of the $k_\perp \rho_s \sim \rho^*$ scaling for the wave vector near the separatrix position in the L-mode, prior to the L-H transition, must be completely ruled out.

The conclusion to be drawn from the above analysis is that the power H-mode threshold must have approximately $P_{thres} \sim R^{1.75}$ or even weaker dependence on R (as the dependence of $k_\perp \rho_s$ on ρ^* is expected to be somewhere between $k_\perp \rho_s = const$ and $k_\perp \rho_s \sim \sqrt{\rho^*}$ possibilities, but seems to be closer to the $k_\perp \rho_s = const$ case), in order to be consistent with the skin effect suppression of the drift wave turbulence as a mechanism for the L-H transition. The dependence $P_{thres} \sim R^{1.75}$ is quite favourable for ITER. Threshold power following from Eq. (8.4) in this case is only 69 *MW* for $\bar{n}_e = 0.5 \times 10^{20} m^{-3}$, $B = 5.68$ *T* and $R = 8.14$ *m*.

9. EFFECT OF HIGH SEPARATRIX T AND β ON THE DISCHARGE PERFORMANCE: DENSITY LIMIT IN ELMY H-MODES

As both the input power and density are raised, the relative weight of the two mechanisms specific to high T and β plasmas should increase, first, near the separatrix. The balance between them must have a profound effect on the overall discharge performance, because they control the L-H transition and cause ELMs. It is of particular interest to have an idea about the relative strength of these two mechanisms in ITER. What will be more important: the stabilising effect of turbulence suppression by large skin times (high T) or the destabilising effect of MHD instabilities (high β)?

To answer this question, criteria (4.5) and (4.10) should first be expressed as ratios (l.h.s. over r.h.s.), to yield threshold parameters:

$$F_{L-H} = \frac{T_e^{13/6}(T_e + T_i)^{1/2}}{B^{4/3}(qR)^{1/3}} \frac{M_{\|}^{1/3}}{z_{eff}} \left(\frac{m_i}{m_D} \right)^{1/6} (f_{k\rho})^{-2/3} , \tag{9.1}$$

$$F_\beta = \frac{qn(T_e + T_i)}{B^2} \left(\frac{T_e + T_i}{T_e} \right)^{1/3} \left(\frac{\rho_s}{qR} \right)^{-2/3} M_{\|}^{1/3} (f_{k\rho})^{1/3}. \tag{9.2}$$

For the radial decay lengths near the separatrix, there may be deviations from the scaling for Δ_{sol} given by Eq. (2.11) which is still employed in the parameters F_{L-H} and F_β (the same remark could be made with respect to all the results on the L-H transition obtained so far). Right at the separatrix, the decay lengths should be affected by both SOL physics and transport processes inside the separatrix. Since, however, the very origin of steep gradients at the separatrix is ultimately due to the particle and heat sinks onto the target, it would be natural to assume that the SOL mechanisms have certain supremacy over those inside the separatrix in establishing the gradients. Another extreme case of the $\lambda_n \sim a$ scaling, which completely ignores the SOL physics, is considered in Section 10.

There is insufficient confidence in the validity of the dependence on q in the beta limit given by Eq. (4.10). On the other hand, the scaling $\nabla\beta \sim 1/R$ for fixed q is quite common to characterise thresholds for MHD phenomena. Since safety factor is about 3 in both ITER and typical JET discharges, in the following analysis q will be assumed fixed.

The net temperature dependence inside the F_β parameter can be eliminated by expressing $(T_e + T_i)$ through F_{L-H} and substituting into F_β, leaving only the dependence on the T_e/T_i ratio. For the case of $f_{k\rho} \equiv k_\perp \rho_s = const$ this gives:

$$F_\beta \sim F_{L-H}^{1/4} \left(\frac{T_e + T_i}{T_e} \right)^{0.88} \frac{nR^{3/4}}{B} z_{eff}^{1/4} M_{\|}^{1/4} \left(\frac{m_i}{m_D} \right)^{-1/24} . \tag{9.3}$$

This formula allows one to establish the ratio of separatrix densities in two different machines that would ensure similar pressure gradients, provided they both operate just above the H-mode power threshold or at a fixed excess of the F_{L-H} parameter over its value corresponding to the L-H transition.

The density in F_β can be replaced with its value normalised to the Greenwald density limit $\bar{n}_e \equiv n_{GW}(m^{-3}) = 10^{14} I_p(A)/\pi a^2(m^2)$ [41]: $K_{GW} = n/n_{GW}$. The dependence of K_{GW} on major radius and toroidal field can be established when this limit is given the form of the Hugill density limit [42] (for the fixed plasma elongation, the functional dependence of the two limits is essentially the same): $n_{GW} \sim n_{Hugill} \sim B/qR$ (q dependence will be ignored). Since the Greenwald limit refers to the line average density, the direct relevance to this limit can only be

made if a fixed proportionality between n_{sep} and $\bar{n}_e$ is assumed. For the case of $k_\perp \rho_s = const$, one obtains:

$$F_\beta \sim F_{L-H}^{1/4} \left(\frac{T_e + T_i}{T_e} \right)^{0.88} \frac{K_{GW} z_{eff}^{1/4} M_\parallel^{1/4}}{R^{1/4}} \left(\frac{m_i}{m_D} \right)^{-1/24} . \qquad (9.4)$$

The physics behind the Greenwald limit has originally been related with the degradation of the core particle confinement and associated increase in power losses at the edge due to convective power flux and/or atomic processes (charge-exchange, ionisation and impurity radiation), as larger fuelling is needed to maintain high density near its limit [41]. This leads to lower edge temperatures which affect current density profile. After the $j_\parallel(r)$ shrinks sufficiently, sharper gradients at the edge will cause instabilities arising from the free energy contained in the poloidal magnetic field, leading to a disruption. Such a scenario seems to be applicable to radiative L-modes. In contrast, in the highest density H-modes in JET and some other machines a “soft”, non-disruptive density limit is observed, with the density rise limited by the degradation in the edge confinement associated with increased ELM frequency [43-45].

In JET, the Greenwald limit can be reached but not exceeded in ELMy H-modes. According to Eq. (9.4), similar problems will be encountered in ITER. The dependence on major radius, however, suggests a possibility of modest improvement in ITER in this respect. For the same F_β as in JET, provided the temperature ratio and other parameters are also the same, K_{GW} in ITER can be increased compared to its value in JET by a factor of $(R_{ITER}/R_{JET})^{1/4} \approx 1.29$ for $R_{ITER}/R_{JET} = 8.14/2.96$. Reducing z_{eff} and the Mach number $M_\parallel$ should also have a beneficial effect. The influence of z_{eff} on the F_β parameter is obvious: according to Eq. (4.5), higher z_{eff} increase the edge T_e necessary to maintain the discharge in the H-mode, and for the same pressure a lower density is permissible. As for the Mach number, its influence has to do with the profile effects. According to Eq. (2.11), larger $M_\parallel$ reduce the SOL width Δ_{sol}, thereby increasing the pressure gradient at the separatrix, so that a smaller separatrix density is permissible for the same F_β. The reduction in $M_\parallel$ can be achieved by increasing recycling in the divertor.

Conclusions about the beneficial role of high recycling in the divertor (provided all other parameters, mainly separatrix T_e and T_i present in F_{L-H} are fixed !) cannot be fully justified within the framework of the present model. The model ignores the effect of neutrals on the main plasma. If the divertor is not closed enough, or there are leaks from the divertor to the main chamber (by-pass leaks), the neutral pressure will increase near the walls, resulting in the cooling of the edge plasma. Whether the ionisation source from these neutrals increases or reduces density gradients near the separatrix, depends on density and temperature distributions across the SOL.

Another deficiency of the present model is its neglect of the electron heat flux through the separatrix. The model predictions, therefore, are better justified when most of the power to the scrape-off layer is supplied through the ion channel, since ion heat conductivity is much more likely to be governed by the same scaling laws as the diffusion coefficient $D_\perp$. Finally, the extremely weak mass-dependence in Eq. (9.4) may not reflect the full extent of possible isotope effect in density limits, since this dependence may be implicitly contained in the magnitude of the $f_{k\rho} \equiv k_\perp \rho_s$ parameter which was supposed to be fixed.

Criterion (4.10) for the onset of the ELM activity does not include any dependence on the collisionality. Experiment, however, seems to suggest that resistivity has a strong impact on ELMs [46]. Therefore, complete similarity of the ELM activity also requires the same $\nu_e^* = z_{eff} nqR/T_e^2$.

For the case of $k_\perp \rho_s = const$, ν_e^* can be expressed as:

$$\nu_e^* \sim F_{L-H}^{-3/4} \left(\frac{T_e + T_i}{T_e} \right)^{0.38} \frac{K_{GW} z_{eff}^{1/4} M_\parallel^{1/4}}{R^{1/4}} \left(\frac{m_i}{m_D} \right)^{1/8}. \tag{9.5}$$

Comparison with Eq. (9.4) shows that F_β and ν_e^* have the same scaling against major radius as well as against z_{eff} and $M_\parallel$. Thus, the maximum density normalised to the Greenwald limit is expected to scale as $R^{1/4}$ for fixed F_{L-H}, T_e/T_i, $n_{sep}/\bar{n}_e$, q, z_{eff} and (here, a "similar" effect of neutrals on the profiles should have been the more appropriate formulation) $M_\parallel$.

For the $k_\perp \rho_s = \sqrt{\rho^*}$ case, the scalings take the form:

$$F_\beta \sim F_{L-H}^{9/20} \left(\frac{T_e + T_i}{T_e} \right)^{1.31} \frac{K_{GW} z_{eff}^{0.45} M_\parallel^{0.18}}{R^{1/2} B^{1/20}} \left(\frac{m_i}{m_D} \right)^{-0.08}, \tag{9.6}$$

$$\nu_e^* \sim F_{L-H}^{-4/5} \left(\frac{T_e + T_i}{T_e} \right)^{0.27} \frac{K_{GW} z_{eff}^{0.2} M_\parallel^{0.27}}{B^{1/5}} \left(\frac{m_i}{m_D} \right)^{0.13}. \tag{9.7}$$

In the ν_e^* dependence, for $B_{ITER}/B_{JET} = 5.68/3.4$ K_{GW} can be increased by 11% in ITER compared to JET, and the collisionality will still be the same in the two machines. At the same time, the scaling of the F_β parameter against major radius is much more favourable for ITER. The factor of access in K_{GW} over JET is 1.70. Since the fundamental source of the ELM instability is the pressure gradient (gradients of current density are the dominant source of MHD instabilities only in "cold" edge plasmas, as in radiative L-modes), the significant reduction of F_β in ITER indicates the possibility of a significantly lower ELM activity. Thus, it appears to be that hopes of exceeding the Greenwald limit in ITER are justified. Since the scaling law for the wave vector should be somewhere between the $k_\perp \rho_s = const$ and $k_\perp \rho_s = \sqrt{\rho^*}$ cases (but more

likely to be biased towards the $k_\perp \rho_s = const$ case), the favourable scaling against major radius suggests a possibility of an increase over the Greenwald limit in ITER by about 30%.

Even larger excess over the Greenwald limit may be possible in ITER if z_{eff} or the temperature ratio T_i/T_e could be reduced (dependencies on $M_\parallel$ and m_i/m_D are more complicated issues as was pointed out earlier). Another way to raise the maximum (core) density is to increase the ratio $\bar{n}_e/n_{e,sep}$ by using pellet injection as has been done in experiments on ASDEX Upgrade [45] and DIII-D [47]. In ASDEX Upgrade, steady state ELMy H-mode discharges with line averaged densities of up to 1.5 of the Greenwald limit were achieved by a combination of repetitive pellet injection with moderate gas puff fuelling [45], despite this machine being much smaller than JET ($R_{JET}/R_{ASDEX-U} = 2.96/1.65$, giving rise to 14% smaller K_{GW} than in JET for "similar" edge parameters, according to Eqs. (9.4-9.5)). This, however, was achieved at the expense of a dramatic reduction in confinement. In DIII-D, line averaged densities of up to 1.4 of the Greenwald limit were achieved. However, good confinement (ITER89P H-factor around 1.75) at such a high densities was maintained only transiently, with radiation rapidly increasing above the input power accompanied by a degradation in confinement.

10. INFLUENCE OF THE $\lambda_n \sim \Delta_{sol}$ ASSUMPTION ON THE MAIN RESULTS

In the previous analysis, the scrape-off layer width Δ_{sol} was used as a characteristic radial decay length near the separatrix. This assumption, as was pointed out in the previous section, is justified by the fact that the very origin of steep gradients near the separatrix is ultimately due to the particle and heat sinks onto the target. Still, transport processes inside the separatrix should definitely have a certain impact on the scaling for decay lengths at the separatrix position. The validity of some important results obtained so far, therefore, may be questioned. This, in particular, applies to the conclusion that ITER will exceed the Greenwald limit. If $k_\perp \rho_s = const$ scaling for the wave vector is adopted, then the validity of this conclusion hinges on a rather weak dependence of the F_β parameter on major radius: $\sim R^{-1/4}$.

In order to check how critically the results obtained depend on the previously made assumptions, it is important to derive scalings for F_{L-H}, F_β, F_P and ν_e^* parameters in another limiting case where the SOL physics is totally ignored: $\lambda_n \sim a$. In the following analysis, the safety factor q, z_{eff} and the Mach number $M_\parallel$ will be assumed fixed, and Δ_{sol} will be replaced with the major radius R. With these assumptions, Eq. (2.13) for the diffusion coefficient should be replaced with:

$$D_\perp \sim c_s \rho_s \frac{1}{f_{k\rho}} \frac{T_e}{T_e + T_i} \frac{\rho_s}{R} \ , \tag{10.1}$$

for fixed $f_{r\theta}$. This results in:

$$D_\perp \sim \frac{T_e\sqrt{T_e+T_i}}{B^2R} \quad \text{and} \quad D_\perp \sim \frac{T_e(T_e+T_i)^{1/4}}{B^{3/2}\sqrt{R}} \tag{10.2}$$

for $k_\perp\rho_s$ =const and $k_\perp\rho_s \sim \sqrt{\rho^*}$ cases respectively. Criterion (4.5) for suppression of drift turbulence by the skin effect, which in effect is the condition on the separatrix parameters prior to the L-H transition, will take the form:

$$F_{L-H} \sim \frac{T_e^{5/2}\sqrt{T_e+T_i}}{B^2R} \quad \text{and} \quad F_{L-H} \sim \frac{T_e^{5/2}(T_e+T_i)^{1/4}}{B^{3/2}\sqrt{R}} \tag{10.3}$$

for $k_\perp\rho_s$ =const and $k_\perp\rho_s \sim \sqrt{\rho^*}$ cases respectively.

The threshold power ratio F_P (Section 8) can be expressed as: $F_P \sim R^{3/2-\gamma}\left[\frac{T_e^{1/3}(T_e+T_i)^{1/6}(T_e+\alpha T_i)^{1/3}}{B\sqrt{R}}\right]^3$, for $k_\perp\rho_s = const$. At the same time, separatrix parameters prior to the L-H transition must satisfy the condition: $\sqrt{F_{L-H}} \sim \frac{T_e^{5/4}(T_e+T_i)^{1/4}}{B\sqrt{R}} = const$. Hence, the $\gamma = 1.5$ assumption is required to make F_P independent of major radius.

For the case of $k_\perp\rho_s \sim \sqrt{\rho^*}$ scaling, F_P can be expressed as: $F_P \sim R^{4/3-\gamma}\left[\frac{T_e^{2/5}(T_e+T_i)^{1/10}(T_e+\alpha T_i)^{2/5}}{BR^{1/3}}\right]^{5/2}$. The L-H transition occurs at $F_{L-H}^{2/3} \sim \frac{T_e^{5/3}(T_e+T_i)^{1/6}}{BR^{1/3}} = const$. Hence, the $\gamma \approx 1.33$ assumption is required to make F_P independent of major radius.

For the ELM activity, the $\lambda_n \sim R$ assumption gives:

$$F_\beta \sim F_{L-H}^{1/3}\left(\frac{T_e+T_i}{T_e}\right)^{0.83}\frac{K_{GW}}{R^{2/3}B^{1/3}} \quad \text{and} \quad F_\beta \sim F_{L-H}^{4/11}\left(\frac{T_e+T_i}{T_e}\right)^{0.91}\frac{K_{GW}}{R^{9/11}B^{5/11}} \tag{10.4}$$

for $k_\perp\rho_s = const$ and $k_\perp\rho_s \sim \sqrt{\rho^*}$ cases respectively. $K_{GW} \equiv n/n_{GW}$ in ITER can be increased significantly compared to JET, by at least a factor of 2.3, for the same F_β.

The scaling for ν_e^* can be expressed as:

$$\nu_e^* \sim F_{L-H}^{-2/3}\left(\frac{T_e+T_i}{T_e}\right)^{0.33}\frac{K_{GW}}{R^{2/3}B^{1/3}} \quad \text{and} \quad \nu_e^* \sim F_{L-H}^{-8/11}\left(\frac{T_e+T_i}{T_e}\right)^{0.19}\frac{K_{GW}}{R^{4/11}B^{1/11}} \tag{10.5}$$

for $k_\perp \rho_s = const$ and $k_\perp \rho_s \sim \sqrt{\rho^*}$ cases respectively.

Compared with the previously analysed case of the $\lambda_n \sim \Delta_{sol}$ scaling, changes in all important critical parameters are beneficial for ITER. The threshold power for the L-H transition, edge pressure gradients and electron collisionality in ITER would only be lower if the decay length λ_n scaled with R, due mainly to favourable scalings against major radius. Positive conclusions about ITER operational space obtained earlier should therefore be regarded as fully justified. At the same time, they are more appropriate for projection to ITER than the results obtained in this section.

CONCLUSIONS

The assumption that drift waves are the fundamental source of turbulence in a typical "cold" and "rare" SOL plasmas (low T and β, but not too high ν^*), combined with experimental results on the relation between perpendicular wave vectors and ion Larmor radius, allows one to derive the diffusion coefficient. The dependence $k_\perp \rho_s = const$ ($\cong 0.2$ as a statistical average), which seems to be supported by observations, results in a near Bohm scaling of the type $D_\perp \sim T^{7/6} B^{-4/3} (qR)^{-1/3}$, being numerically close to the Bohm diffusion coefficient for typical edge parameters. An insistence on the exact Bohm-type scaling requires $k_\perp \rho_s \sim \sqrt{\rho^*}$. Reality must be somewhere between these two possibilities. Validity of Bohm- and near Bohm-type scalings must break down in "very cold" plasmas (Eq. (3.6) gives an absolute minimum for the temperature threshold). Collisionality controls dynamics of the combined drift and interchange instability in such plasmas, and ν^* is an important parameter.

Finite β effects reveal themselves through MHD instabilities caused by the pressure gradient (increases with β) and by the skin effect. The *collisional* skin effect, caused by Spitzer conductivity, can be characterised by the dimensionless combination $\beta \varepsilon q \rho^{*-2} \nu^{*-1}$ in the main plasma, and, being proportional to $T^2 a$, physically is controlled by temperature. Since drift turbulence is accompanied by fluctuating parallel currents, the skin effect is capable of reducing its level by splitting wide flux tubes. The skin frequency for the drift fluctuations with the radial displacement Δ is: $\nu_{skin} = c^2 / 8\sigma\Delta^2$ ($k_r >> k_\theta$ and $\Delta = \pi / k_r$ are assumed here). At low T_e, the frequency of the drift fluctuations ν is much lower than ν_{skin}. The critical temperature for the onset of a strong influence of the skin effect on the drift turbulence corresponds to $\nu = \nu_{skin}$. This equality can also be expressed as $D_\perp \equiv \Delta^2 \nu = c^2 / 8\sigma$ - the condition for equal rates of the plasma diffusion into the magnetic field and the diffusion of the magnetic field into the plasma. The same criterion can be derived by equalising the *collisional* skin-depth $\Delta_{coll.skin} = \sqrt{c^2 / 8\sigma\nu}$ to the radial displacement Δ. For $T_e > T_{e,crit}$, the size of the fluctuations Δ is limited by $\Delta_{coll.skin}$

and the relation $D_\perp = c^2/8\sigma$ is observed. Owing to $\sigma \sim T_e^{3/2}$, the diffusion coefficient decreases with temperature as $D_\perp \sim T_e^{-3/2}$, in contrast with the increase according to Bohm- or near Bohm-type scalings at low T_e.

The dependence $D_\perp(T_e)$, therefore, is non monotonic. Once the critical T_e at its peak is reached, first near the separatrix (reasons why the separatrix should be a favourite location for this event are given in Section 5), drift turbulence can be suppressed by the skin effect and the temperature may have a sudden upward excursion. The time scale for fast profile re-adjustments within the layer of the order of the fluctuation size is ~80 ms for $T_e = T_i = 100$ *eV* and $B = 3$ *T* in JET. This is interpreted as the L-H transition. The analysis yields $T_e^{13/8}(T_e+T_i)^{3/8}/B(qR)^{1/4}$ as a critical parameter for the L-H transition for the $k_\perp\rho_s$ =*const* scaling for the wave vector of the fluctuations ($T_e^{13/6}(T_e + T_i)^{1/3}/B$ for the $k_\perp\rho_s \sim \sqrt{\rho^*}$ case). In dimensional space, the bifurcation is attributed to the involvement of two dimensionless parameters in the L-H transition physics: ρ^* and $\beta/\nu^*\rho^{*2}$.

Another necessary condition for the suppression of turbulence is that the *collisionless* skin-depth $\Delta_{skin} \sim c/\omega_{p_e} \sim 1/\sqrt{n_e}$, being the lower limit of distances controlled by the *collisional* skin effect, must be smaller than the size of drift fluctuations in the L-mode: $\Delta_{drift} \sim k_\perp^{-1} \sim \rho_s \sim \sqrt{T}/B$ ($k_\perp\rho_s = const$ is assumed here). The requirement $\Delta_{skin} < \Delta_{drift}$ imposes a restriction on minimum β which, when combined with the temperature threshold for the L-H transition, defines a lower density threshold for the L-H transition. Increase in the critical pedestal T_e often observed in experiments at low densities should be related (at least partly) with approaches to the density threshold. Near this threshold, turbulent displacements in the L-mode phase prior to the L-H transition are close to the collisionless skin-depth. The electron parallel conductivity in these conditions is reduced by electrons' inertia, and higher T_e is required to cause the transition.

The mechanism of the drift turbulence suppression by the skin effect implies such a relation between T_e, T_i, B, q, R and n_e at the separatrix prior to the L-H transition that ensures consistency between the experimentally found H-mode power threshold of the type $P_{thres} \sim n_e B R^\gamma$ and dimensionally correct scaling $P_{thres} \sim R^2 \times n_e D_\perp (T_e + \alpha T_i)/\Delta_{sol}$. Once this mechanism is adopted as an explanation of the L-H transition, it clarifies the uncertainty over the value of the power γ in the P_{thres} dependence on major radius existing in the present multi-machine database on the L-H transition. This coefficient must be: $\gamma \approx 1.75$, or even lower. According to dimensionally correct scaling developed by the ITER Confinement Database and Modelling Expert Group, $\gamma = 1.75$ corresponds to the threshold power of less than 70 *MW* for $\bar{n}_e = 5 \times 10^{19} m^{-3}$.

The critical parameter for the L-H transition (F_{L-H}), together with dimensionless parameters characterising the pressure gradient (F_β) and the resistivity (ν_e^*), create the set of similar-

ity parameters describing ELM behaviour. The scaling for the separatrix density normalised to the Greenwald density limit $n_{e,sep}/n_{GW}$ with the machine size and toroidal field which ensures "similar" ELM behaviour can thus be obtained. For the fixed similarity parameters, the analysis yields weak ($\sim R^{1/4}$) but favourable dependence of $n_{e,sep}/n_{GW}$ on the major radius. In recent experiments on JET and other machines, the degradation in the edge confinement associated with increased ELM frequency was found to be responsible for the density limit in high power H-modes. Owing to the approximately $R^{1/4}$ dependence, an excess over the Greenwald limit, $\bar{n}_e/n_{GW}$, by about 30% higher in ITER compared to JET for "similar" conditions (q, $n_{e,sep}/\bar{n}_e$, separatrix z_{eff} and the T_e/T_i ratio, wall conditions, the use of pellets etc.) in ELMy H-modes is predicted. This is with the provision that a limit on the central density, related to mechanisms in the plasma core, is not encountered.

ACKNOWLEDGEMENTS

The author is indebted to G.F.Matthews for his significant contribution to this work. Helpful discussions with J.W.Connor, M.Endler, S.K.Erents, M.Gryaznevich, Yu.L.Igitkhanov, G.Janeschitz, W.Kerner, A.Loarte, V.V.Parail, O.P.Pogutse, G.Saibene, B.Scott, P.C.Stangeby and K.Thomsen are greatly acknowledged.

REFERENCES

[1] Kadomtsev B.B., Sov. J. Plasma Phys. 1 (1975) 295.
[2] Lackner K., Comments Plasma Phys. Control. Fusion 13 (1990) 163.
[3] Lackner K., Comments Plasma Phys. Control. Fusion 15 (1994) 359.
[4] Hutchinson I.H. and Vlases G.C., Nucl. Fusion 36 (1996) 783.
[5] Catto P.J., Krasheninnikov S.I. and Connor J.W., Phys. Plasmas 3 (1996) 927.
[6] Connor J.W. and Taylor J.B., Nucl. Fusion 17 (1977) 1047.
[7] Nedospasov A.V., Sov. J. Plasma Phys. 15 (1989) 659.
[8] Endler M., Niedermeyer H., Giannone L. et al., Nucl. Fusion 35 (1995) 1307.
[9] Liewer P.C., Nucl. Fusion 25 (1985) 543.
[10] Shaing K.C. and Crume E.C., Jr., Phys. Rev. Lett. 63 (1989) 2369.
[11] Biglary H., Diamond P.H. and Terry P.W., Phys. Fluids B 2 (1990) 1.
[12] Itoh K. and Itoh S.-I., Plasma Phys. Control. Fusion 38 (1996) 1.
[13] Kotschenreuther M., Dorland W., Liu Q.P. et al., 16th IAEA Fusion Energy Conf., Montreal, Canada, 7-11 October 1996, paper IAEA-CN-64/D1-5.
[14] "ITER L-mode Confinement Database", Kaye S.M. and the ITER Confinement Database Working Group, submitted to Nucl. Fusion.
[15] ITER H-mode Database Working Group, Nucl. Fusion 34 (1994) 131.

[16] Callen J.D., Phys. Rev. Letters 39 (1977) 1540.
[17] Kerner W., Pogutse O., JET-P(96) 24, submitted to Nucl. Fusion (letters).
[18] Sykes A., Turner M.F. and Patel S., Proc. of the 11th Euro. Conf. on Control. Fusion and Plasma Phys. (Aachen 1983), Vol. 2, p. 363.
[19] Troyon F., Gruber R., Saurenmann H., Semenzato S. and Succi S., Plasma Phys. Control. Fusion 26 (1984) 209.
[20] Scott B., Camargo S., Jenko F., 16th IAEA Fusion Energy Conf., Montreal, Canada, 7-11 October 1996, paper IAEA-CN-64/DP-18.
[21] Rogers B.N., Drake J.F., Lau Y.T., Guzdar P.N., Hassam A.B., Novakovski S.V. and Zeiler A., 16th IAEA Fusion Energy Conf., Montreal, Canada, 7-11 October 1996, paper IAEA-CN-64/D1-4.
[22] Erents S.K., Breger P., Davies S.J. et al., in the Proceedings of the 12th PSI Conference (St.Raphael, May 20-24, 1996), paper A09, to be published in J. Nucl. Mater.
[23] LaBombard B., Goetz J.A., Hutchinson I.H. et al., 16th IAEA Fusion Energy Conf., Montreal, Canada, 7-11 October 1996, paper IAEA-CN-64/AP2-5.
[24] Fishpool G., presented at Task Force “D” meeting at JET on 20/11/1995.
[25] Kadomtsev B.B., Sov. J. Plasma Phys. 13 (1987) 443.
[26] Neudatchin S.V., Cordey J.G., Muir D.G., (1993), JET-P(93)58.
[27] Romanelli F., Tang W.M. and White R.B., Nucl. Fusion 26 (1986) 1515.
[28] Rebut P.H., Lallia P., Watkins M., Proc. 12th Int. Conf. Plasma Phys. and Controlled Fusion Research, Nice, France, 1988, Vol. 2, p.191.
[29] Connor J.W., Hastie R.J., Taylor J.B., Proc. Roy. Soc. London Ser. A 365, 1 (1989).
[30] Romanelli F., Zonca F., Phys. Fluids B 5 (1993) 4081.
[31] Parail V.V., Cherubini A., Erba M. et al., “Numerical Analysis of the Heat Pulses in JET”, to be published in Proc. 23rd Euro. Conf. on Control. Fusion and Plasma Phys. (Kiev, 1996).
[32] Hubbard A.E., Goetz J.A., Greenwald M. et al., 16th IAEA Fusion Energy Conf., Montreal, Canada, 7-11 October 1996, paper IAEA-CN-64/AP2-11.
[33] Zohm H., Suttrop W., de Blank H.J. et al., 16th IAEA Fusion Energy Conf., Montreal, Canada, 7-11 October 1996, paper IAEA-CN-64/AP-1.
[34] Groebner R.J., Carlstrom T.S., Burrell K.H. et al., 16th IAEA Fusion Energy Conf., Montreal, Canada, 7-11 October 1996, paper IAEA-CN-64/AP2-10.
[35] Righi E., Bickley A., Campbell D.J. et al., “Dedicated ITER H-mode Power Threshold Experiments in JET”, submitted to Plasma Phys. Control. Fusion.
[36] Hinton F.L., Nucl. Fusion 25 (1985) 1457.
[37] Chankin A.V. and Stangeby P.C., Plasma Phys. Control. Fusion 38 (1996) 1879.
[38] ITER Confinement Database and Modelling Expert Group (Presented by T.Takizuka), 16th IAEA Fusion Energy Conf., Montreal, Canada, 7-11 October 1996, paper IAEA-CN-

64/F-5.
[39] Fukuda T., Sato M., Takizuka T. et al., 16th IAEA Fusion Energy Conf., Montreal, Canada, 7-11 October 1996, paper IAEA-CN-64/AP2-9.
[40] McCormick G.K., Chankin A., Clement S. et al., in the Proceedings of the 12th PSI Conference (St.Raphael, May 20-24, 1996), paper A11, to be published in J. Nucl. Mater.
[41] Greenwald M., Terry J.L., Wolfe S.M. et al., Nucl. Fusion 28 (1988) 2199.
[42] Stott P.E., Hugill J., Fielding S.J. et al., in Contr. Fusion and Plasma Phys. (Proc. 8th Euro. Conf. Prague, 1979), Vol. 1, European Physical Society (1979) 151.
[43] Saibene G., Campbell D., Horton L.D. et al., in the Proceedings of the 12th PSI Conference (St.Raphael, May 20-24, 1996), paper A16, to be published in J. Nucl. Mater.
[44] Petrie R.W., Kellman A.G., Ali Mahdavi M., Nucl. Fusion 33 (1993) 929.
[45] Kaufmann M., Schweinzer J., Albrecht M. et al., 16th IAEA Fusion Energy Conf., Montreal, Canada, 7-11 October 1996, paper IAEA-CN-64/O1-5.
[46] Lingertat J., private communication.
[47] Maingi R., Mahdavi M.A., Jernigan T.C. et al., “Investigation of physical processes limiting plasma density in high confinement mode discharges on DIII-D”, submitted to Phys. Plasmas.

APPENDIX 1: COLLISIONAL DRIFT AND INTERCHANGE INSTABILITIES

Analysis of individual instabilities in collisional plasmas can be found in [Kadomtsev B.B.,

Pogutse O.P., in “Reviews of Plasma Physics”, Consultants Bureau, New-York - London, Vol.5 (1970) pp.296-303], as well as many other sources.

In light of a special importance attached to drift and interchange instabilities in the SOL, it is worth giving a brief guidance through physical mechanisms responsible for these instabilities. For simplicity, only the density gradient as a source of an instability will be considered. Inclusion of temperature gradients does not lead to any new quality essential for dimensional analysis.

Suppose a radial displacement of the plasma at some point has created a bulge on the line of constant density. Such a perturbation will usually be stretched along the field lines, with $\lambda_{||} \le 2\pi qR$, so that there exist small parallel gradients of density. On the figure, the profile of the bulge is continued by dashed lines to reflect a conventional approximation of all perturbations by $\exp[i(\mathbf{kr} - \omega t]$ in the slab geometry. The radial structure of the bulge (wave vector k_r) is not reflected in the figure but will be accounted for in equations.

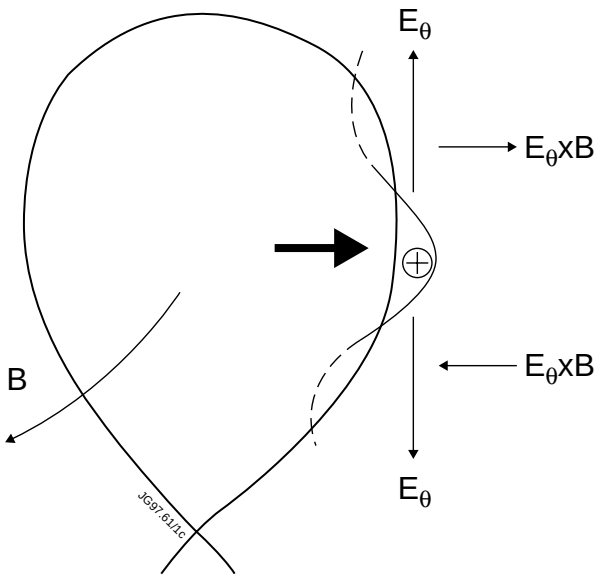

At the centre of the bulge the electric potential has a maximum, to compensate for the parallel electron pressure gradient (electrons obey Boltzmann distribution in the absence of friction), provided electrons move fast enough along the field lines to react on changes in the electric potential: $v_e >> \omega/k_{||}$. Finite parallel wavelength is essential for Boltzmann distribution of electrons, so that they could move away from the bulge along the field lines. On the other hand, ions should not be too fast to escape the bulge along the field lines, so that it would quickly disappear: $c_s << \omega/k_{||}$. Thus, the restriction on the parallel phase velocity will be: $c_s << \omega/k_{||} << v_e$ (the condition $v_i << \omega/k_{||}$ is also required to avoid strong kinetic mechanism for the wave damping: Landau damping).

The poloidal electric field has its maximum and minimum on the fringes of the bulge, whereas $E_\theta = 0$ in its centre. Therefore, $E_\theta \times B$ drift will be shifting the two sides of the bulge in opposite directions radially, and the whole structure will effectively move up. This is a drift wave; it propagates in the electron diamagnetic direction. Whether the size of the bulge will grow as it moves, is determined by mechanisms which affect changes in the amplitude of E_θ acting across the bulge (δE_θ) and shown on the following figures.

Ion inertia leads to the so called drift instability. Heavier ions are slightly shifted along oscillating $\mathbf{E}_\perp$ in phase with $\dot{\mathbf{E}}_\perp \equiv d\mathbf{E}_\perp/dt$, in addition to their $\mathbf{E}\times\mathbf{B}$ drift. The resultant current (the polarisation drift) is given by: $\mathbf{j}_\perp = nm_i c^2 \dot{\mathbf{E}}_\perp / eB^2$.

As the bulge propagates like a wave over the plasma, the phase of the poloidal current ($\sim \dot{E}_\theta$) is such that it peaks at the centre of the bulge, while being zero at its fringes. Therefore, $div_\theta j_\theta$ will pump a negative charge to the top and positive - to the bottom of the bulge (assuming a sinusoidal wave: j_θ is reversed at the centres of the two neighbouring "anti-bulges" depicted by dashed lines on the first figure). The sign of the variation in the poloidal electric field δE_θ is such that the bulge should grow. The rate of growth will depend on the magnitude of δE_θ. If the ion-electron friction is negligible, the charges will escape along the field lines without creating significant magnitude of δE_θ. Collisionality, therefore, does not lead to the dissipation of the bulge, but, on the contrary, facilitates its further growth.

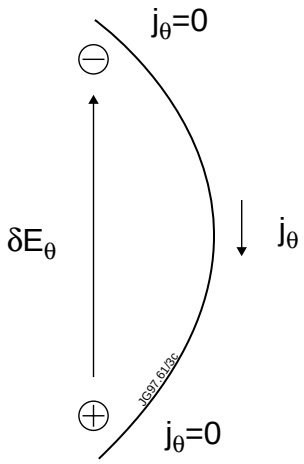

ion inertia

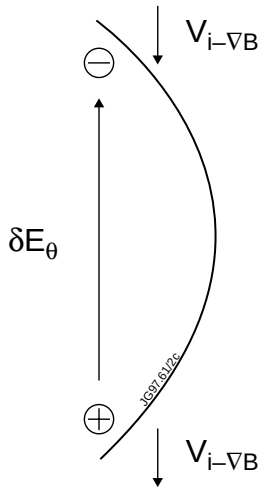

∇B–drift

Vertical ∇B drift is responsible for the interchange instability. At the outer midplane, ∇B drift is exactly in the poloidal direction. Opposite directions of this drift for ions and electrons result in the net current density of their Larmor circles: $j_y \approx \pm 2n\left(T_e + T_i\right)/BR$. Owing to the poloidal variation of density created by the bulge, j_θ is not poloidally constant and $div_\theta j_\theta$ will pump a positive charge to the bottom and negative - to its top fringe. Again, as in the previous example, δE_θ causes growth of the bulge. The same arguments applied to a bulge localised near the inner midplane would create the same direction of δE_θ (upward), but there the $E_\theta \times B$ drift acts so as to eliminate the bulge. That is why the interchange instability has positive growth rates on the outboard and negative - on the inboard sides of the magnetic surface.

Finally, there exists the effect of finite ion Larmor radius which tends to stabilise the instabilities. It requires the inclusion of the radial structure (finite k_r) of the mode in the analysis. Large Larmor radius of ions slightly averages the E_θ acting on the whole Larmor circle, so

that the $\mathbf{E}\times\mathbf{B}$ drift velocity for ions will be smaller than that for electrons giving rise to the net current density $\mathbf{j}_\perp = -Sen\,c[\mathbf{E}\times\mathbf{B}]/B^2$, where $S = k_\perp^2 T_i / m_i\omega_i^2$ and $k_\perp \equiv \sqrt{k_x^2 + k_y^2}$.

In the linear approximation, perturbations of the electric potential are assumed to be small: $\tilde{\varphi}/eT_e << 1$. This also implies small perturbations of density, $\tilde{n}$, and electric field, $\tilde{\mathbf{E}} = -\nabla\tilde{\varphi} = -i\mathbf{k}\tilde{\varphi}$ (all perturbations have an $\exp[i(\mathbf{kr} - \omega t]$ structure with different phases). Expressions for all three contributions to the perpendicular current should be linearised (products $\tilde{n}\tilde{\varphi}$ etc. are neglected) and substituted into the quasi-neutrality equation: $div\mathbf{j} = 0$ ($k_r\tilde{j}_r + k_\theta\tilde{j}_\theta + k_\parallel\tilde{j}_\parallel = 0$). This gives for the individual contributions to the parallel current: $\tilde{j}_\parallel = k_\perp^2/k_\parallel \cdot nm_ic^2/B^2 \cdot \omega\tilde{\phi}$ for the polarisation drift, $\tilde{j}_\parallel = \tilde{n}k_\theta/k_\parallel \cdot 2(T_e + T_i)/BR$ for the ∇B drift, and $\tilde{j}_\parallel = -ik_\theta Sec/Bk_\parallel \cdot \tilde{\varphi} \cdot dn/dr$ for the effect of a finite ion Larmor radius.

Perturbations $\tilde{n}$ and $\tilde{\varphi}$, as well as ω and components of the wave vector, figure in the expressions for $\tilde{j}_\parallel$, whereas the objective is to find the $\omega(\mathbf{k})$ dependence. There are two equations to attain it. Parallel electron equilibrium equation reads:

$$-\partial p_e/\partial s_\parallel - enE_\parallel + j_\parallel m_e\nu_{ei}/e = 0. \qquad \text{(A1.1)}$$

All three $\tilde{j}_\parallel$ are to be summed up and substituted into the linearised form of this equation:

$$-ik_\parallel\tilde{n}T_e = i\cdot enk_\parallel\tilde{\varphi} + \tilde{j}_\parallel m_e\nu_{ei}/e. \qquad \text{(A1.2)}$$

Density perturbations are described by the continuity equation:

$$\partial n/\partial t + div\left(nc\mathbf{E}\times\mathbf{B}/B^2\right) = 0. \qquad \text{(A1.3)}$$

Its linearised form is: $\tilde{n} = -k_\theta\tilde{\varphi}c/\omega B \cdot dn/dr$. It allows one to replace $\tilde{n}$ with $\tilde{\varphi}$ in the parallel electron equilibrium equation. After such a replacement and cancellation of $\tilde{\varphi}$, the dispersion equation will be obtained:

$$\omega^2 + i\cdot\alpha\omega\omega_d + i\cdot\omega\omega_s - i\cdot\omega_d\omega_s \pm \omega_o^2\left(k_\theta/k_\perp\right)^2 = 0\ . \qquad \text{(A1.4)}$$

Here $\omega_d = k_\theta cT_e/eB\lambda_n$ is the angular frequency of the drift wave, also responsible for the polarisation drift (ion inertia) giving rise to the drift instability; $\omega_o^2 = 2(T_e + T_i)/m_iR\lambda_n$ describes the effect of the vertical ∇B drift, leading to the interchange instability at the outer midplane (sign "+"), or stabilisation of turbulence at the inner midplane (sign "-"); $\omega_s = \omega_i\omega_e/\nu_{ei}\cdot k_\parallel^2/k_\perp^2$ characterises the ability of spatial charge to diffuse along the field lines without creating perturbations of electric potential (proportional to ν_{ei}^{-1}); $\alpha = T_i/T_e$.

APPENDIX 2: SCALINGS FOR $D_\perp$ AND Δ_{sol} FOR DIFFERENT DEPENDENCIES OF $k_\perp\rho_s$ ON ρ^*

Adopting any particular form of the dependence $k_\perp\rho_s \sim (\rho^*)^\alpha$ for different α gives rise to different scalings for $D_\perp$ both in the main plasma and in the SOL. For the frequency of fluctuations, the assumption that turbulence consists of drift waves gives:

$$\omega \sim \frac{k_\perp T}{B \times (size)}, \tag{A2.1}$$

where the characteristic radial size should be taken as minor radius a for the core and Δ_{sol} - for the scrape-off layer. An expression for the SOL width contains the diffusion coefficient:

$$\Delta_{sol} \sim (D_\perp qR/\sqrt{T})^{1/2}. \tag{A2.2}$$

In order to find both Δ_{sol} and $D_\perp$, another equation which relates the diffusion coefficient with $k_\perp$ and the frequency should be used:

$$D_\perp \sim \omega/k_\perp^2 \ . \tag{A2.3}$$

These three equations allow one to obtain the following scalings:

$k_\perp\rho_s$	ρ^*	$\sqrt{\rho^*}$	*const*	$1/\sqrt{\rho^*}$	$1/\rho^*$
core $D_\perp$	$\frac{T}{B}\frac{qR}{a}$	$\frac{T^{5/4}}{B^{3/2}}\frac{\sqrt{qR}}{a}$	$\frac{T^{3/2}}{B^2}\frac{1}{a}$	$\frac{T^{7/4}}{B^{5/2}}\frac{1}{a\sqrt{qR}}$	$\frac{T^2}{B^3}\frac{1}{aqR}$
SOL $D_\perp$	$\frac{T^{5/6}}{B^{2/3}}(qR)^{1/3}$	$\frac{T}{B}$	$\frac{T^{7/6}}{B^{4/3}}\frac{1}{(qR)^{1/3}}$	$\frac{T^{4/3}}{B^{5/3}}\frac{1}{(qR)^{2/3}}$	$\frac{T^{3/2}}{B^2}\frac{1}{qR}$
Δ_{sol}	$\frac{T^{1/6}}{B^{1/3}}(qR)^{2/3}$	$\frac{T^{1/4}}{B^{1/2}}(qR)^{1/2}$	$\frac{T^{1/3}}{B^{2/3}}(qR)^{1/3}$	$\frac{T^{5/12}}{B^{5/6}}(qR)^{1/6}$	$\frac{T^{1/2}}{B}$

The most probable cases for the ρ^* scaling are in the fourth ($k_\perp\rho_s \sim const$) and third ($k_\perp\rho_s \sim \sqrt{\rho^*}$) columns, the former corresponding to the gyro-Bohm scaling for $D_\perp$ in the core. The q-dependencies will change for all the cases apart from $k_\perp\rho_s \sim const$ when $\rho^* \sim \sqrt{T}/RB$ is adopted instead of $\rho^* \sim \sqrt{T}/qRB$.